Two Approaches for the Prediction of Plume-Induced Separation

J. H. Fox
Calspan Corporation, AEDC Division

April 1985

Final Report for Period October 1982 — January 1984

ARNOLD ENGINEERING DEVELOPMENT CENTER
ARNOLD AIR FORCE STATION, TENNESSEE
AIR FORCE SYSTEMS COMMAND
UNITED STATES AIR FORCE

NOTICES

When U. S. Government drawings, specifications, or other data are used for any purpose other than a definitely related Government procurement operation, the Government thereby incurs no responsibility nor any obligation whatsoever, and the fact that the government may have formulated, furnished, or in any way supplied the said drawings, specifications, or other data, is not to be regarded by implication or otherwise, or in any manner licensing the holder or any other person or corporation, or conveying any rights or permission to manufacture, use, or sell any patented invention that may in any way be related thereto.

Qualified users may obtain copies of this report from the Defense Technical Information Center.

References to named commercial products in this report are not to be considered in any sense as an endorsement of the product by the United States Air Force or the Government.

This report has been reviewed by the Office of Public Affairs (PA) and is releasable to the National Technical Information Service (NTIS). At NTIS, it will be available to the general public, including foreign nations.

APPROVAL STATEMENT

This report has been reviewed and approved.

Robert H. Nichols

ROBERT H. NICHOLS
Directorate of Technology
Deputy for Operations

Approved for publication:

FOR THE COMMANDER

Marion L. Laster

MARION L. LASTER
Director of Technology
Deputy for Operations

UNCLASSIFIED

SECURITY CLASSIFICATION OF THIS PAGE

REPORT DOCUMENTATION PAGE

1a REPORT SECURITY CLASSIFICATION UNCLASSIFIED	1b RESTRICTIVE MARKINGS
2a SECURITY CLASSIFICATION AUTHORITY	3 DISTRIBUTION/AVAILABILITY OF REPORT Approved for public release; distribution unlimited.
2b DECLASSIFICATION/DOWNGRADING SCHEDULE	
4 PERFORMING ORGANIZATION REPORT NUMBER(S) AEDC-TR-84-18	5 MONITORING ORGANIZATION REPORT NUMBER(S)
6a NAME OF PERFORMING ORGANIZATION Arnold Engineering Development Center 6b OFFICE SYMBOL (If applicable) DOF	7a NAME OF MONITORING ORGANIZATION
6c ADDRESS (City, State and ZIP Code) Air Force Systems Command Arnold Air Force Station, TN 37389-5000	7b ADDRESS (City, State and ZIP Code)
8a NAME OF FUNDING/SPONSORING ORGANIZATION Arnold Engineering Development Center 8b OFFICE SYMBOL (If applicable) DOT	9 PROCUREMENT INSTRUMENT IDENTIFICATION NUMBER
8c ADDRESS (City, State and ZIP Code) Air Force Systems Command Arnold Air Force Station, TN 37389-5000	10 SOURCE OF FUNDING NOS PROGRAM ELEMENT NO: 63370F PROJECT NO TASK NO WORK UNIT NO
11 TITLE (Include Security Classification) See Reverse of This Page	
12 PERSONAL AUTHOR(S) Fox, J.H., Calspan Corporation, AEDC Division	
13a TYPE OF REPORT Final 13b TIME COVERED FROM 10/1/82 TO 1/1/84	14 DATE OF REPORT (Yr, Mo, Day) April 1985 15 PAGE COUNT 58
16 SUPPLEMENTARY NOTATION Available in Defense Technical Information Center (DTIC).	

17 COSATI CODES			18 SUBJECT TERMS (Continue on reverse if necessary and identify by block number)
FIELD	GROUP	SUB GR	
16	04		separation Navier-Stokes equations computational fluid dynamics
16	02		

19. ABSTRACT (Continue on reverse if necessary and identify by block number)

A comparison with available measured data is presented of the numerically predicted location of plume-induced separation on the afterbody of a bluff-base missile configuration at supersonic speed. A modified version of the implicit, three-dimensional Pulliam-Steger thin-layer Navier-Stokes code was used. The principal modification is the coupling of an inviscid algorithm to the viscous method to overcome the nozzle-lip difficulty encountered with highly underexpanded nozzles. This modification allowed the relatively easy computation of the interaction resulting from jet-to-free-stream static pressure ratios through fifteen. In comparison with the measured data, the predictions of the separation locations are very good through a pressure ratio of 9.2. At a pressure ratio of fifteen, the method underpredicted the extent of separation.

20 DISTRIBUTION/AVAILABILITY OF ABSTRACT UNCLASSIFIED/UNLIMITED ☐ SAME AS RPT ☒ DTIC USERS ☐	21 ABSTRACT SECURITY CLASSIFICATION UNCLASSIFIED
22a NAME OF RESPONSIBLE INDIVIDUAL W. O. Cole	22b TELEPHONE NUMBER (Include Area Code) (615) 455-2611 Ext. 7813 22c OFFICE SYMBOL DOS

DD FORM 1473, 83 APR EDITION OF 1 JAN 73 IS OBSOLETE

UNCLASSIFIED

SECURITY CLASSIFICATION OF THIS PAGE

TITLE. Continued.

Two Approaches for the Prediction of Plume-Induced Separation

PREFACE

The work reported was conducted by the Arnold Engineering Development Center (AEDC), Air Force Systems Command (AFSC), under AEDC Project No. D205PW. The analysis was done at the request of the AEDC Analysis and Evaluation Division (DOFA) for AEDC/DOT. The AEDC/DOT project manager was Dr. Keith Kushman, and the AEDC/DOFAA project manager was Mr. Russell B. Sorrells. The results were obtained by Calspan Corporation, AEDC Division, operating contractor of the Aerospace Flight Dynamics testing effort at the AEDC, AFSC, Arnold Air Force Station, Tennessee. The manuscript was submitted for publication on April 26, 1984.

CONTENTS

ILLUSTRATIONS

Figure Page

APPENDIX

1.0 INTRODUCTION

As aircraft become capable of sustained flight at higher altitudes, their rocket-propelled weapons are being subjected to environments at launch and boost which were not anticipated when these weapons were designed. Of particular importance is the phenomenon of plume-induced separation. Such separation, if severe, can subject control surfaces to low-speed recirculating flows which may seriously degrade the effectiveness of the surface. A simple calculation may determine that separation could not occur, for instance, if the nozzle exit pressure is less than or equal to free stream. However, if it is determined that the nozzle is highly underexpanded, i.e., the jet-to-free-stream static pressure ratio is greater than six, then the determination of whether separation is occurring to such an extent as to cause difficulties requires either wind tunnel testing with a real plume or a numerical solution of the equations that closely describe the flow. This report details the development of two predictive techniques: one a component method, where the inviscid and viscous parts of the flow are treated separately and coupled at their interfaces, and the other a Navier-Stokes (N-S) method.

Figure 1 is a schematic of a representative afterbody flow with plume-induced separation. The separation occurs because the afterbody flow must compress to turn outward around the plume. When the adverse pressure gradient is larger than that which enables attached flow, the afterbody flow lifts off. When the detached flow reattaches at the plume, it turns through a further compression, causing a secondary shock which coalesces with the separation shock and forms a lambda shock pattern. The plume boundary also turns and another shock is formed which finally coalesces with the barrel shock of the plume. This complex of shocks is known in component methods as the trailing shock system. Within the separated layer, a low-speed recirculating flow exists. In the component method this region is usually assumed to be at constant pressure. This is because most measured data show a distinct pressure profile shape along the afterbody that increases abruptly through the compression and reaches a level that is fairly flat relative to the initial compression. The pressure changes little until very near reattachment on the jet plume. The mathematical description of such a viscous interaction is provided by the Navier-Stokes equations.

Although computational costs are declining, routine solution of the Navier-Stokes equations is still not practical. It is therefore important to explore the capabilities of existing approximate techniques, determine their accuracy, and determine their extent of applicability. The initial phase of this work was thus directed toward developing and

extending an existing component method that had proved to work well in predicting base properties where separation on the afterbody was not present. A requirement arose, however, for a predictive technique for vehicles at high angles of attack. The component methods are not applicable in these flows, because they require an external criterion for separation that is based on singular point separation, which is no longer valid in three-dimensional flows (Ref. 1). This led to the modification of a three-dimensional N-S solver specifically to solve the plume-induced separation problem. This work with the N-S solver allowed it to be brought into use when another drawback to the component method became apparent: at low free-stream Mach number and high jet-to-free-stream pressure ratios, the external flow is forced to turn beyond the supersonic turning limit, causing a detached normal shock. The component method was not formulated to account for mixed flows.

This report is of two parts. The first part presents the approach to developing the component method into a tool for predicting plume-induced separation. The second part is devoted to the modifications required of a three-dimensional N-S solver to make it useful for predicting plume-induced separation at realistic jet-to-free-stream pressure ratios.

2.0 COMPONENT METHOD

2.1 GENERAL

The development of a component method capable of predicting plume-induced separation is based on previous work, Refs. 2-4, which had generalized and extended the basic mixing and base flow theory of A. J. Chapman and H. H. Korst, Refs. 5-6, for predicting base properties. This generalized theory was proved capable of predicting base flows, taking into account the boundary layer existing at separation, base bleed, and the interaction of gas streams differing in chemistry and total enthalpy. Because of the wealth of literature on this method, this report will dwell only on the changes required of the theory as developed in Ref. 3.

2.2 BASIC COMPONENT THEORY

The basic component method based on Korst's work contains three distinct analyses: an inviscid analysis is used to determine the overall flow structure and the pressure field; a second analysis generates a set of integral conservation equations which describe the viscous flow into and out of the base region; and the final analysis develops the mixing theory which produces the flow property profiles across the shear layers. Each of these analyses may be developed independently. They are coupled in an iterative process. A solution to the base flow problem is achieved when the set of integral conservation equations is satisfied.

At any step in the iterative process, the base properties serve as boundary conditions to the inviscid set of equations and to the mixing model. The base pressure adjusts the boundaries of the converging inviscid streams, the mixing theory locates the mixing profiles on the inviscid boundaries, and the integral conservation equations balance the energies and mass rates into and out of the base region. The residual error of the integral conservation equations drives the iteration process.

For the method to have closure, certain key streamlines must be located within the shear layers, Figs. 2 and 3. The most difficult, historically, to determine is the stagnation streamline, which determines what part of the converging shear layers will turn back toward the base and what part will be turned downstream to experience recompression. There are many theories available for determining this streamline, all using empirical data to locate the stagnation point. The methods of Refs. 3 and 4 use a minimum of empirical information to develop a very workable theory that has been tested without change over a wide range of flow configurations, including flows with enthalpy and chemistry differences at widely different Mach numbers.

The coordinate systems used in the component method are sometimes confusing. The general coordinate system is axially symmetric with X being the axial coordinate and R the radial coordinate; however, the mixing layers have their own system. The coordinate along the longitudinal direction of the shear layer is ℓ; $\ell = 0$ at the point of separation. Y is the coordinate normal to ℓ, and X is the coordinate along the slip surface where the two streams converge after separation (see Fig. 3).

2.3 EXTENSION OF THEORY

The analysis of Ref. 4 is extended in a straightforward manner to account for separation occurring upstream of the base-afterbody juncture. This involves a modification to the inviscid flow solver (method of characteristics) to accommodate the separation shock wave, as illustrated in Fig. 2, and the inclusion of a separation criterion. Hahn, Ruppert, and Mahal (Ref. 7) reviewed existing criteria extensively to determine when separation occurs. For turbulent free-interaction separation, the authors suggest the criterion proposed by Reshotko and Tucker

$$M_2/M_1 = 0.762 \tag{1}$$

That is, separation will occur when the ratio of the Mach number downstream of the separation shock to that upstream of the shock is equal to 0.762. This criterion is particularly easy to apply; however, its main drawback is that the separation on a boattail afterbody is not truly of the free-interaction type. The upstream influence of the changing curvature of the body is not taken into account. It would be expected that separation

predictions would be more accurate for large separations where the point of separation is well up on the body.

2.4 MIXING THEORY

As shown in Fig. 2, the separated region is bounded by two shear layers which are assumed to converge at a slipline. The slipline is determined from the axially symmetric, rotational method of characteristics (MOC). The method of characteristics is used also to determine the inviscid, constant pressure boundaries of the separated region. At the inviscid intersection, point I, the two mixing layers are assumed to have known velocity profiles:

$$\phi = \frac{1}{2}\left[1 + \operatorname{erf}\left(\eta - \eta_p\right)\right] + \frac{\eta_p}{\sqrt{\pi}} \int_0^{1.0} \zeta_i^{1/n} e^{-(\eta - \eta_p \zeta)^2} d\zeta \tag{2}$$

where $\zeta_i^{1/n}$ is the initial boundary-layer power-law profile and

$$\eta = \frac{\sigma Y}{\ell} \tag{3}$$

and

$$\eta_P = \frac{\sigma \delta}{\ell} \tag{4}$$

where σ is the mixing parameter. Equation (2) is the widely used error function profile distorted by the initial boundary layer. As the boundary-layer thickness goes to zero, the second term becomes negligible. This occurs both when the separating boundary layer is very thin and when the distance from separation to reattachment is large, i.e., as ℓ becomes large. When η_p becomes small, the mixing layer is considered fully developed. The mixing parameter σ is determined semiempirically. The method of Ref. 8 shows it to be well approximated by

$$\sigma = \int_{\eta_L}^{\eta_D} \frac{\frac{\varrho}{\varrho_U} \phi^2 d\eta}{\left[C_k \left(\frac{d\phi}{d\eta}\right)_D^2\right]} \tag{5}$$

where C_k is given as $0.5085/\sigma_o$. In the present work the incompressible σ_o is taken as 9.0.

Each profile at point I has the transverse coordinate η normal to its respective inviscid boundary, increasing in value toward the high-speed stream. Following Ref. 6, the Y = 0 point is located by a momentum balance as

$$\int_0^{Y_U} \varrho u^2 dY \Big|_{\ell = 0} = \int_{Y_L}^{Y_U - Y_M} \varrho u^2 dY \Big|_{\ell} \tag{6}$$

This relation is solved for Y_M. This increment is the distance from the inviscid boundary to the zero point of the profile. Thus this relation locates the profiles relative to their inviscid boundaries. The edges of the mixing zones are somewhat arbitrary, but the points that have worked well over many conditions are determined by the following:

1. Y_U is located where the velocity is 99.998895 percent of the high-speed value.
2. Y_L is located at the point where the velocity is 0.001105 percent of the high-speed value.

Two streamlines must now be identified before the conservation relations for the base flow may be presented. The first, the dividing streamline, is defined as

$$\int_0^{Y_U} \rho u dY \Big|_{t=0} = \int_{Y_D}^{Y_L} \rho u dY \Big|_{t} \tag{7}$$

This relation is solved for the location Y_D of the dividing streamline. It is that location in the profile outside ("outside" considered as toward the high-speed edge) of which the mass of the just-separated flow is accounted for. The second streamline is the stagnating streamline which is located in the profile at Y_S. As stated earlier, this streamline divides the mixing layer into the parts that either turn back toward the base or have enough energy to proceed downstream through recompression. Locating this streamline requires a theory of recompression as outlined in the following.

2.5 RECOMPRESSION

Korst's original theory assumed that the stagnating streamline had a stagnation pressure equal to the static pressure downstream of the recompression shock. This was shortly found to be incorrect by Korst and others. (It has become nearly a liturgical requirement of any critical discussion of Korst's theory to dismiss his theory because of this initial assumption which, of course, has nothing to do with a basic theory that has proved its usefulness if by nothing more than its longevity.) The actual pressure is somewhat less than the peak pressure. A procedure for determining this pressure and thus the stagnating streamline was developed in Refs. 3 and 4 and is summarized here.

In the process of computing the inviscid fields, the trailing shock system is also computed. The trailing shock system shown in Fig. 2 also determines the angle of the slipline which serves as the convergence surface for the two shear layers. Its computation is straightforward. The relations

$$\frac{\lambda}{u}\Big|_{S1} = \frac{\lambda}{u}\Big|_{S2} \tag{8}$$

and

$$p_{S1} = p_{S2} \tag{9}$$

must be satisfied along the slipline. These two relations, coupled with the oblique shock relations for the two streams, are sufficient for determining the slipline position and angle.

The recompression is assumed to stretch from X_1 to X_2 (see Fig. 3) and to follow the functional form (Ref. 3)

$$\frac{p - p_B}{p_r - p_B} = \sin^2\left[\left(\pi/2\right)\frac{X - X_1}{X_2 - X_1}\right] \tag{10}$$

where the variable X is incremented along the slipline. The location X_1 is the beginning of recompression and X_2 the end. (Note that recompression is assumed to occur on both sides of the slipline, each recompression process independent of the other and coupled only by the common static pressure of the base region and the common pressure downstream of the trailing shock system.)

The location of X_1 is found geometrically by making the angles β_1 and β_2 equal. The location of X_2 is found with the expression

$$\int_{X_1}^{X_2} pR\,dX = \sin\gamma\overline{R}\int_{Y_1}^{Y_U + Y_m} \varrho u^2\,dY + p_B(R_U + R_1)\,(X_U - X_1)/2 \tag{11}$$

which is developed in Ref. 3 from a momentum balance of the oncoming shear layer with the pressure force on the slipline. The radial effect has been taken into account because of the sometimes significant change in radius along the slipline (the radial effect in the mixing layer is relatively minor). The stagnating streamline is assumed to come to rest isentropically. Thus sufficient information is developed to determine the location of the stagnating streamline. For example, an isoenergetic perfect gas gives

$$\phi_S^2 = \frac{1 - (p_B/p_s)^{(\gamma - 1)/\gamma}}{1 - (p_B/p_{T_U})^{(\gamma - 1)/\gamma}} \tag{12}$$

The geometry of the profile relative to the slipline and Eqs. (10) - (12) completely determine the location Y_S of the stagnating streamline.

2.6 CONSERVATION EQUATIONS OF THE BASE FLOW

With the key streamline locations, Y_{S1}, Y_D, and Y_S known, it is possible to set down the basic mass and energy balance relations. For the conservation of mass,

$$\int_{Y_L}^{Y_D} \rho u dY \Big|_{S1} + \int_{Y_L}^{Y_D} \rho u dY \Big|_{S2} = \int_{Y_L}^{Y_S} \rho u dY \Big|_{S1} + \int_{Y_L}^{Y_S} \rho u dY \Big|_{S2} \quad (13)$$

and for energy,

$$\int_{Y_L}^{Y_S} \rho u H dY \Big|_{S1} + \int_{Y_L}^{Y_S} \rho u H dY \Big|_{S2} = H_B \left(\int_{Y_L}^{Y_D} \rho u dY \Big|_{S1} + \int_{Y_L}^{Y_D} \rho u dY \Big|_{S2} \right) \quad (14)$$

These constitute the primary equations which are solved for the properties in the base/separated region. Several auxiliary relations may be used when a species difference exists between the exhaust gas and the free stream. These are found in Ref. 3 and are not detailed here.

2.7 INITIAL VELOCITY PROFILE

The theory as developed in Refs. 3 – 4 assumed that the separating layer off a bluff base would have a power-law profile. For separation occurring upstream of the base, the separating profile is more closely related to the wake-like profile of a developing shear layer as shown in Fig. 4, using data from Refs. 9 – 10. This shape develops in a shear layer from an initial power-law profile some distance downstream of a bluff edge. To more closely model the shape of the separating profile, the separating layer is assumed to separate with a profile with $\eta_p = 4.0$. Thus, in the present calculations, it is assumed that the distance ℓ has been extended by a virtual amount. Thus the effective mixing length is

$$\ell_{eff} = \ell + \ell_{vir} \quad (15)$$

where

$$\ell_{vir} = \sigma\delta/4.0 \quad (16)$$

2.8 COMPUTATIONAL PROCEDURE

Initial calculations were done using the GASL method of characteristics program, Ref. 11. This code was found to convect total pressure loss from the bow shock too far into the field of the afterbody. This caused an overprediction of the extent of separation at higher Mach numbers. The present results were calculated by assuming a constant pressure equal to the free-stream pressure from the shoulder of the missile to just upstream of the boattail break. Boundary-layer growth was then determined over this length using the method of Ref. 12. The solution procedure is then as follows for isoenergetic flows:

1. The MOC of Ref. 3 is started assuming free-stream conditions with no boundary-layer displacement taken into account. This computation is marched downstream to an assumed point of separation.

2. A separation shock wave is computed and the MOC is continued. The boundary on the edge of the separated region is determined by the guess of pressure in that region. Computation of the plume field is also done with the MOC. The intersection of the plume and outer stream is found and used to determine the length of the inviscid boundaries.

3. The trailing shock system and slip surface are computed to obtain the peak recompression pressure.

4. The viscous mixing theory is then applied and the key streamlines are determined. Finally, a mass balance of flow into and out of the separated region is made.

If the mass balance equation is not satisfied, an error is determined, a new pressure is calculated, and steps 2 through 4 are repeated. Once a converged separation pressure is determined, the separation criterion for a turbulent boundary layer, Eq. (1), is used to determine whether separation has occurred. If this condition is not satisfied, a new separation point is assumed, and steps 1 through 4 are repeated. This continues until a separation point is determined.

2.9 DISCUSSION OF COMPONENT METHOD RESULTS

Experimental data for afterbodies with a plume-induced separation are not widely available. However, two reports of measured data that have appeared in the literature are sufficient for validating the method as an engineering tool (Refs. 13 and 14). The results from Ref. 13 are from a configuration run at a free-stream Mach number of 3.5 at various static jet-to-free-stream pressure ratios. Comparisons are presented in Fig. 5 of predictions made using the present component method with the measured data. Actual measured separation points are not presented as they were not available; however, the predicted separation point, which is indicated by the step rise in pressure, is located at a position within the pressure rise that is consistent with the beginning of separation from other data that are available, i.e., Ref. 14. They show separation occurring 10 to 20 percent into the pressure rise. The calculated plateau pressure is high compared to the measured data. This is because the predicted pressure is that which occurs downstream of an inviscid oblique shock wave, which is of zero thickness. The measured pressure on the afterbody, however, is the result of the smearing effect of the viscous layer, which spreads out the compression. The peak pressure is thus pushed downstream, perhaps off the body.

Comparison was made with the data of Ref. 14 at a lower Mach number. This comparison is shown in Fig. 6. At the lower pressure ratios, the comparison is quite poor. In general, the component method gives quite acceptable results at high jet-to-free-stream pressure ratios where the separation is greater than three nozzle radii up the afterbody from the base. This is expected since the external criterion used to determine when separation is occurring is based on free interaction separation where separation is based only on local conditions free from direct influences of downstream geometry such as the afterbody/base juncture.

An anomalous condition sometimes occurs when trying to predict separation on bodies where the Mach number of the outer stream is significantly lower than the Mach number of the expanded jet boundary at the slipline. If the pressure ratio of the jet to free stream is sufficiently high, then a solution to the trailing shock problem cannot be obtained because the outer stream is required to turn further than the oblique shock limit. That is, the recompression shock on the plume boundary must be detached. This means that a subsonic region exists downstream of the detached shock wave. The basic theory of this component method does not account for such flows; therefore, this type of flow must be treated by other methods, i.e., Navier-Stokes methods. This condition played substantially in the decision to pursue the Navier-Stokes methods as discussed in the following.

3.0 THE NAVIER—STOKES APPROACH

3.1 GENERAL

There are two principal reasons for exploring the use of N-S solvers for the solution of the plume-induced separation problem:

1. The occurrence of the detached shock at the plume boundary with its attendant subsonic region invalidates the component method because of its use of a spatially hyperbolic inviscid solver (MOC). This happens when the two streams are of substantially different Mach numbers.

2. A requirement for predictions at very high angles of attack (10 to 20 deg) also invalidates the component method, because its externally applied separation criterion is based on the occurrence of singular type separation, which does not occur in general in three-dimensional flows.

A third, but less justifiable, reason is the fact that N-S solvers are conceptually pleasing because they use fewer empirically determined constructs. That element of the method which does require empiricism, the modeling of the turbulent viscosity, shows signs of becoming a rapidly maturing technology (Refs. 15 - 16).

When the N-S solver was used as detailed here, it became apparent early that extensive modification of the code would be required, if the extent of separation at any jet-to-free-stream pressure ratio of interest was to be computed. The difficulty arises in the region just downstream of the nozzle lip. At high-pressure ratios, the barrel shock of the plume begins to form, developing a region of very high gradients. The expansion from the nozzle overshoots, causing the local pressure to be lower than the ambient pressure. The flow must then be compressed sharply through the mechanism of the barrel shock to the boundary pressure. The usual method of overcoming this type of problem is to either concentrate the computational mesh in this region or add additional smoothing or do both. The adding of points quickly reaches a limit when the available memory in the computer is exhausted and the resolution of other important features of the flow is seriously degraded. Smoothing fails for an interesting reason. Smoothing effectively increases the viscosity in the high gradient region. This has the effect of over-entraining fluid from the region of the base just above the nozzle lip to the point that the pressure becomes unrealistically low, often to the point of being negative, causing the time-marching scheme to fail. If heroic measures are taken to prevent the low pressure, the converged solution will often lack sufficient predictive accuracy. For these reasons, an artifice was developed to circumvent the nozzle-lip problem.

Because of the behavior of the algorithm in the nozzle-lip region and from experience derived from development of the component model discussed earlier, the interaction at the nozzle lip was determined to be primarily inviscid. The nozzle lip is thus treated inviscidly and removed from the region of the viscous solver. The inviscid MOC is used to develop new boundary conditions for the N-S solver downstream of the nozzle lip.

Results are presented of comparisons with available experimental data using this new procedure. A study using the same measured data for comparison was done by Deiwert, Ref. 17. He used an azimuthally invariant form of the equations and a different gridding philosophy.

In the following, since the numerical tools are well developed and readily available in the open literature, many of the details will be referenced.

3.2 BASIC EQUATIONS

The three-dimensional, unsteady, thin-layer Navier-Stokes equations are transformed (see Appendix A) into the curvilinear coordinate system ξ, η, ζ, and τ as

$$\partial_\tau \hat{q} + \partial_\xi \hat{E} + \partial_\eta \hat{F} + \partial_\zeta \hat{G} = R_e^{-1} \partial_\zeta \hat{S} \tag{17}$$

where, with reference to Fig. 1, ξ is the body-conforming coordinate in the streamwise direction, η is the body-conforming coordinate in the azimuthal direction, and ζ is the outward coordinate ray from the body to the outermost boundary. The Cartesian x coordinate is the axis of the body, the z coordinate is normal to x and tangent to the base of the body, and the x-z plane forms the slice used for presentation. Thus the Cartesian velocity components of interest are u and w. The vectors $\hat{q}$, $\hat{E}$, $\hat{F}$, and $\hat{G}$ are

$$\hat{q} = J^{-1}\begin{vmatrix} \rho \\ \rho u \\ \rho v \\ \rho w \\ e \end{vmatrix} \qquad \hat{E} = J^{-1}\begin{vmatrix} \rho U \\ \rho uU + \xi_x p \\ \rho vU + \xi_y p \\ \rho wU + \xi_z p \\ (e + p)U - \xi_t p \end{vmatrix} \tag{18}$$

$$\hat{F} = J^{-1}\begin{vmatrix} \rho V \\ \rho uV + \eta_x p \\ \rho vV + \eta_y p \\ \rho wV + \eta_z p \\ (e + p)V - \eta_t p \end{vmatrix} \qquad \hat{G} = J^{-1}\begin{vmatrix} \rho W \\ \rho uW + \zeta_x p \\ \rho vW + \zeta_y p \\ \rho wW + \zeta_z p \\ (e + p)W - \zeta_t p \end{vmatrix} \tag{19}$$

$$\hat{S} = J^{-1}\begin{vmatrix} 0 \\ \mu(\zeta_x^2 + \zeta_y^2 + \zeta_z^2)u_\zeta + (\mu/3)(\zeta_x u_\zeta + \zeta_y v_\zeta + \zeta_z w_\zeta)\zeta_x \\ \mu(\zeta_x^2 + \zeta_y^2 + \zeta_z^2)v_\zeta + (\mu/3)(\zeta_x u_\zeta + \zeta_y v_\zeta + \zeta_z w_\zeta)\zeta_y \\ \mu(\zeta_x^2 + \zeta_y^2 + \zeta_z^2)w_\zeta + (\mu/3)(\zeta_x u_\zeta + \zeta_y v_\zeta + \zeta_z w_\zeta)\zeta_z \\ \Big\{(\zeta_x^2 + \zeta_y^2 + \zeta_z^2)\big[0.5\mu(u^2 + v^2 + w^2)_\zeta \\ + k\,Pr^{-1}(\gamma - 1)^{-1}(a^2)_\zeta\big] + (\mu/3)(\zeta_x u + \zeta_y v + \zeta_z w) \\ \times(\zeta_x u_\zeta + \zeta_y v_\zeta + \zeta_z w_\zeta)\Big\} \end{vmatrix} \tag{20}$$

and the contravariant velocities are

$$\begin{aligned} U &= \xi_t + \xi_x u + \xi_y v + \xi_z w \\ V &= \eta_t + \eta_x u + \eta_y v + \eta_z w \\ W &= \zeta_t + \zeta_x u + \zeta_y v + \zeta_z w \end{aligned} \tag{21}$$

The pressure is determined from

$$p = (\gamma - 1)[e - 0.5\varrho(u^2 + v^2 + w^2)] \tag{22}$$

and the Cartesian velocity components are non-dimensionalized with the free-stream speed of sound a_∞; density ϱ is scaled by ϱ_∞; and the total energy, e, by $\varrho_\infty a_\infty^2$.

The chain rule expansion of derivatives of the Cartesian coordinates with respect to the curvilinear coordinates is solved to give the metric terms

$$\begin{aligned}
\xi_x &= J(y_\eta z_\zeta - y_\zeta z_\eta) & \eta_x &= J(z_\xi y_\zeta - y_\xi z_\zeta) \\
\xi_y &= J(z_\eta x_\zeta - x_\eta z_\zeta) & \eta_y &= J(x_\xi z_\zeta - x_\zeta z_\xi) \\
\xi_z &= J(x_\eta y_\zeta - y_\eta x_\zeta) & \eta_z &= J(y_\xi x_\zeta - x_\xi y_\zeta) \\
\zeta_x &= J(y_\xi z_\eta - z_\xi y_\eta) & \xi_t &= -x_\tau \xi_x - y_\tau \xi_y - z_\tau \xi_z \\
\zeta_y &= J(x_\eta z_\xi - x_\xi z_\eta) & \eta_t &= -x_\tau \eta_x - y_\tau \eta_y - z_\tau \eta_z \\
\zeta_z &= J(x_\xi y_\eta - y_\xi x_\eta) & \zeta_t &= -x_\tau \zeta_x - y_\tau \zeta_y - z_\tau \zeta_z
\end{aligned} \tag{23}$$

with

$$J^{-1} = x_\xi y_\eta z_\zeta + x_\zeta y_\xi z_\eta + x_\eta y_\zeta z_\xi - x_\xi y_\zeta z_\eta - x_\eta y_\xi z_\zeta - x_\zeta y_\eta z_\xi \tag{24}$$

The approximate factorization difference equation is

$$\begin{aligned}
&(I + h\delta_\xi \hat{A}^n - \epsilon_I J^{-1} \nabla_\xi \Delta_\xi J)(I + h\delta_\eta \hat{B}^n - \epsilon_I J^{-1} \nabla_\eta \Delta_\eta J) \times \\
&(I + h\delta_\zeta \hat{C}^n - hR_e^{-1} \delta_\zeta J^{-1} \hat{M}^n J - \epsilon_I J^{-1} \nabla_\zeta \Delta_\zeta J)(\hat{q}^{n+1} - \hat{q}^n) \\
&\quad = -\Delta t (\delta_\xi \hat{E}^n + \delta_\eta \hat{F}^n + \delta_\zeta \hat{G}^n - Re^{-1} \delta_\zeta \hat{S}^n) \\
&\quad - \epsilon_E J^{-1} \left[(\nabla_\xi \Delta_\xi)^2 + (\nabla_\eta \Delta_\eta)^2 + (\nabla_\zeta \Delta_\zeta)^2\right] J\hat{q}^n
\end{aligned} \tag{25}$$

where the δ's are the central-difference operators, Δ and ∇ are forward and backward difference operators, and $h = t/2$. The matrices $\hat{A}^n$, $\hat{B}^n$, and $\hat{C}^n$ are obtained from the linearization in time of $\hat{E}^n$, $\hat{F}^n$, and $\hat{G}^n$. These are detailed by Pulliam and Steger, Ref. 18, along with the coefficient matrix $\hat{M}^n$. The smoothing terms of the forms $\epsilon_I J^{-1} \nabla_\xi \Delta_\xi J\hat{q}$ and

ϵ_E J^{-1} $(\nabla_\xi \Delta_\xi)^2$ $J\hat{q}$ are added specifically to damp nonlinear instabilities of the central difference scheme.

This algorithm has been put into a practical code by Pulliam and Steger. The actual code used herein is a vectorized form of Pulliam and Steger's code developed by J. A. Benek.

3.3 GRID

The development of a grid for the computational domain is perhaps as important as the solution algorithm itself. Because the thin-layer form of the conservation equations is being used, certain physical assumptions are carried with any choice of grid.

The principal assumption made in the choice of grid is that the wake flow downstream of the base region including the plume may be treated as an inviscid, rotational flow. It is also assumed that the boundary layer in the nozzle has little effect on separation and may be neglected. The effluent from the nozzle is thus treated as an inviscid, conical flow.

These basic assumptions lead to the backward "c" grid as shown in Fig. 7. By wrapping the afterbody/base region in a body-conforming coordinate, the basic code is left unchanged; concentrations of rays may be easily positioned at the nozzle lip region where resolution is most important, and the rays can be readily aligned with the plume boundary so that the reattachment point and the trailing shock system may be better resolved. Since the thin-layer assumption retains only those viscous terms in the conservation equations that have derivatives in the ζ direction and since the ζ coordinate is nearly aligned with the principal flow direction, the viscous terms effectively eliminated are in the region downstream of the base/afterbody juncture.

The grid is wrapped in opposite directions away from the nozzle lip with an exponentially increased spacing. A radius equal to 10 percent of the nozzle radius is added at the juncture of the base and the afterbody to smooth the grid around this corner. Axially symmetric flow is enforced by using five planes with identical boundary conditions. Five planes are required because of the fourth-order smoothing required for stability of the algorithm, Eq. (25). Early experimentation with underexpanded nozzles led to a device to avoid the singularity at the nozzle lip. Without extremely dense packing of points in the lip region, no flow with pressure ratios of significance could be computed. Consequently, the nozzle lip was eliminated from the region of computation for the viscous code. This was accomplished by adding a new surface extending from just above the nozzle lip to the nozzle centerline, as shown in Fig. 8.

3.4 BOUNDARY CONDITIONS AND NOZZLE-LIP ARTIFICE

The Pulliam-Steger-Benek N-S solver uses explicit boundary conditions. While it is arguable that this type boundary condition impedes convergence, it nevertheless provides an extremely practical code in which boundary conditions may be easily input or modified as were done on the new surface that avoids the nozzle-lip problem.

The boundary conditions on the new surface are provided by the MOCs (see Ref. 3), as shown in Fig. 9. Beginning with the exit plane conditions, the steady, Euler-equations MOC is used to march an inviscid field out to the new boundary. The nozzle-lip singularity is treated as a multivalued point using a Prandtl-Meyer centered expansion. The flow at the lip is expanded until it reaches the pressure of the base point that is the intersection of the new boundary and the base. As the base pressure changes continuously from initial conditions to the final converged solution, the expansion is adjusted with each time step. The boundary conditions of the Navier-Stokes solver are thus being adjusted with each step. The boundary conditions on the new surface that are imposed on the Navier-Stokes solver are obtained from the characteristics by a double linear interpolation: i.e., the first interpolation is performed as the characteristics cross the new boundary, and the second is done to find the flow properties at the fixed grid of the Navier-Stokes solver. The MOC develops its own grid from the initial spacing in the nozzle exit plane and from the number of pressure decrements through the expansion. So, a finer grid spacing in the nozzle exit plane or in the expansion will increase the resolution on the boundary for the N-S solver. A finer expansion grid is required for the higher pressure ratios.

The boundary conditions elsewhere are imposed in a straightforward manner. On the body, the no-slip conditions are enforced with the contravariant velocities set to zero. Density is imposed on the body as a first-order extrapolation from the first grid point off the body. Adiabatic wall conditions are enforced with the total energy, e, determined from the zero pressure gradient condition normal to the wall. The upstream boundary-layer profile is taken from the experimental data. Free-stream conditions are imposed at the outer boundary from the upstream boundary to the coordinate ray through the afterbody/base juncture, where the condition is changed to a zero-gradient outflow condition from that point to the centerline. The conditions between the last streamline of the expansion fan and the base are obtained by first-order extrapolation from the field.

3.5 TURBULENCE MODEL

For N-S solvers to be useful in predicting flow behavior for practical configurations, they require a turbulence model to relate properties of the flow field to the apparent change in

in viscosity caused by turbulence. The algebraic models are most attractive because of their simplicity.

Baldwin and Lomax, Ref. 15, developed an algebraic turbulent viscosity model that is widely used because of its favorable trade-off between ease of use and predictive accuracy in unseparated flows. This model is a two-layer model with the inner mixing length proportional to the product of distance from the wall and the Van Driest damping factor. It crosses over to a wake-type model in which the mixing length is scaled by the vorticity. According to Ref. 15, the model is valid for separated flows and, with the outer model alone, for pure wakes. However, Thomas (Ref. 19) reports that if the outer model alone is used for wakes, instabilities develop, and that Baldwin, in private communication with Thomas, recommended using the basic two-layer model with minor adjustment. Thomas proceeded, however, to develop his own variant. But for the present work, it was determined from numerical experiments that the basic Baldwin-Lomax two-layer model, with minor change, worked quite well.

The eddy viscosity is defined as

$$\epsilon_{in} = \varrho \ell^2 \mid \omega \mid \tag{26}$$

near the body. It is defined in the wake as

$$\epsilon_{out} = KC_{cp}\, \varrho\, F_{wake}\, F_{kleb}\,(y) \tag{27}$$

The inner model is switched over to the wake model when $\epsilon_{in} = \epsilon_{out}$. The variable y here refers to normal distance from the body and

$$\mid \omega \mid = \left[\left(\partial_y u - \partial_x v\right)^2 + \left(\partial_z v - \partial_y w\right)^2 + \left(\partial_x w - \partial_z u\right)^2 \right]^{1/2} \tag{28}$$

and

$$\ell = ky \left[1 - \exp\left(\frac{-y+}{A+} \right) \right] \tag{29}$$

where

$$y+ = y \left[\frac{(\varrho\tau)^{1/2}}{\mu} \right]_{wall} \tag{30}$$

Also,

$$F_{kleb}\,(y) = \left[1 + 5.5 \left(\frac{C_{kleb}\, y}{y_{max}} \right)^6 \right]^{-1} \tag{31}$$

and

$$F_{wake} = y_{max} F_{max} \tag{32}$$

or

$$F_{wake} = C_{wk} y_{max} U_{dif}^2 F_{max} \tag{33}$$

depending on which is the smaller. The terms y_{max} and F_{max} are determined from the maximum of the function

$$F(y) = y \mid \omega \mid \left[1 - \exp\left(\frac{-y+}{A+}\right)\right] \tag{34}$$

Also,

$$U_{dif} = (u^2 + v^2 + w^2)^{1/2} - (u^2 + v^2 + w^2)^{1/2}. \tag{35}$$

Baldwin and Lomax assigned the following values to the parameters:

$$\begin{aligned} A+ &= 26.0 \\ C_{cp} &= 1.6 \\ C_{kleb} &= 0.3 \\ C_{wk} &= 0.25 \\ k &= 0.4 \\ K &= 0.0168 \end{aligned} \tag{36}$$

3.6 TURBULENCE MODEL VERIFICATION

Numerical experiments were performed for the configuration shown in Fig. 10 to evaluate the two-layer model in separated flow. This configuration of an afterbody and solid plume simulator was tested in the Acoustic Research Tunnel (ART) at AEDC, Ref. 20. As shown in Fig. 10, the pressure distribution and the separation point prediction were improved significantly if it were assumed that the boundary layer, after separation, became essentially free of turbulent stress. A similar observation was made by Swanson, Ref. 21, relative to solutions of the Navier-Stokes equations about a configuration very similar to the ART model. He found that a relaxation turbulence model suggested by Shang and Hankey,

Ref. 22, improved his results significantly. According to Swanson, this was because the eddy viscosity was decreased in the outer (separated) layer, which served to decrease the plateau pressure, bringing it into better agreement with measurements. Good results were obtained with the ART model by restricting the turbulent viscosity to the region near the body no larger than the attached, upstream, in-flow boundary-layer thickness. As a practical matter, this was accomplished by terminating the calculation of turbulent viscosity at the grid point away from the body surface nearest the thickness of the boundary layer. A family of pressure distribution curves between the upper and lower curves of Fig. 10 may be calculated by varying the point of termination of turbulence from the thickness of the boundary layer to the width of the entire field. No calculations were made with the turbulence turned off any closer to the body than the boundary-layer thickness. Because of these findings, the turbulence was calculated only out to the thickness of the upstream boundary layer in the comparisons with the FFA measurements that follow.

Since these numerical experiments with the Baldwin-Lomax model were conducted, a new model has been introduced by Johnson and King, Ref. 16, that promises to overcome the above difficulties. The model predicts more accurately the apparent viscosity in the outer region of the separating boundary layer and, according to the paper, gives excellent predictions of the pressure distribution in the separated region.

3.7 COMPUTED RESULTS AND COMPARISONS WITH MEASURED DATA

The method was applied to a configuration run by Agrell and White, Ref. 14, as shown in Fig. 11, where the unit Reynolds number is $195{,}000/R_N$, R_N is 15 mm, and the afterbody boundary-layer shape is the 1/7 power-law profile.

The configuration with a boattail of 8 deg was chosen because it was the one for which the most results were shown in Ref. 14. The initial conditions used were free stream everywhere with the upstream boundary-layer profile and thickness assumed along the entire body-conforming coordinate. The nozzle exit conditions were set to the correct Mach number for a conical flow nozzle, but the exit static pressure was initially set equal to the ambient pressure. After approximaely 300 time steps, the nozzle exit pressure was increased in stages up to the static jet-to-free-stream pressure ratio of interest. The maximum pressure ratio of the experiments was 15.2. No upper limit to pressure ratio was determined; however, the higher pressure ratios were more difficult to obtain because smaller time steps had to be used to assure convergence. Achieving a higher pressure ratio using a converged solution as a starting point was usually more difficult than beginning from the initial conditions and stepping the pressure every few hundred time steps.

The results and comparisons are presented in Figs. 11-20. The predicted point of separation on the afterbody is compared with the measured results in Fig. 11. The comparison is very good at the lower pressure ratios with a gradual underprediction noticeable as the pressure ratio passes through twelve. This underprediction is attributed to the decrease in grid resolution on the plume boundary at the reattachment point, because an increase in the pressure ratio lifts the plume boundary out of the finer mesh region. This situation could be helped by using an adaptive grid.

Also in Fig. 11 is the separation curve computed using the Chapman-Korst component method as described previously and shown in Fig. 6. It shows poor agreement for the lower pressures. This is caused by the method's reliance on theory developed for free-interaction separation before a forward facing step. This theory does not account for the effect of the afterbody shape with bluff base on separation. Thus when the separation becomes quite large, the base effects being propagated upstream are diminished and agreement improves. The Chapman-Korst component method is used at the AEDC as a quick screening method to detemine whether separation could be a problem.

Figure 12 presents the comparison with experiment of the afterbody pressure distribution. The predicted pressure distribution shows good agreement, except for the plateau region. However, if the first peak is compared with the experimental plateau pressures as in Fig. 13, the agreement is good. The dip in the pressure curve after the first peak appears to be attributable to the lack of grid resolution and to the radius inserted in the base/afterbody juncture.

The base pressure shows poor agreement with measured data as shown in Fig. 14. The base pressure has a fairly large variation on the bluff face. This is caused both by the base corner radius and by the displaced boundary at the nozzle lip. No experimentation was performed to determine the smallest radius allowable by the method. It is apparent from calculations made on different configurations that this radius is much too large for the base size. This size has caused the recirculating eddies to be displaced, causing, in turn, the pressure disparity. Calculations made with different configurations also show that if sufficient flat base area is maintained relative to the corner radius and the displaced boundary, a typical flat pressure distribution on the face is obtained. Experimentation with the position of the intersection of the displaced boundary and the base area showed that moving the point changed the local base pressure, but not the position of separation.

The contour plots of density and static pressure in Figs. 15 - 18 show the computed features of the entire field. The lambda shock structure is readily apparent, and it is particularly sharply defined in the pressure contour plot at a pressure ratio of six. As the

pressure ratio is changed from six to 15.2, the separation location, as indicated by the separation shock, moves upstream. The trailing shock structure, however, is not well-resolved.

Figures 19 and 20 show further the amount of information provided by the method. They are plots of velocity vectors. Separated areas are easily identified by the abrupt change in velocity on the afterbody.

Converged predictions of separation location were achieved in approximately 2,100 sec of CRAY-1S processing time for each case presented. Significant changes in separation location cease after about 1,800 sec.

In summary, a thin-layer, implicit Navier-Stokes method was used to solve the plume-induced separation problem. To achieve high static jet-to-free-stream pressure ratios, the nozzle lip was removed from the region of the viscous solution and solved inviscidly as a centered expansion. The predictions were very good, except at the highest pressure ratios, where underprediction of separation apparently resulted from poor grid resolution. It was also demonstrated that the thin-layer approximation is legitimate for calculating large separated flow regions if care is taken with the turbulence model, and that the near wake could be treated adequately if considered as being largely devoid of viscous effects. The method demonstrated a marked improvement in accuracy over the Chapman-Korst component method, achieving a predictive accuracy sufficient to allow the method to be used as an engineering tool. Also, it permits solutions of plume interference problems in the flow regimes where the Chapman-Korst component method fails. The accuracy of this approach is expected to improve with improved grid resolution when larger computer memory becomes available.

4.0 CONCLUSIONS AND RECOMMENDATIONS

Two methods for determining the extent of plume-induced separation on afterbodies in supersonic flow have been developed. The first, a Chapman-Korst component method that uses an external separation criterion, produces quite good predictions at very high jet-to-free-stream pressure ratios where extensive separation is present. It does not predict small separation regions well, and it fails when the trailing shock system has embedded subsonic flow. However, because of its speed and relative ease of use, coupled with the fact that it will predict the type of separation that could blank a control surface, it is the first choice for quick screening of possible effects of chamber pressure and afterbody design.

The second method presented requires the solution of the thin-layer Navier-Stokes equations. This method shows its strength in these very flow regimes where the component

method fails, i.e., regimes where the extent of separation is relatively small and regimes where extensive subsonic flow occurs. The thin-layer form of the equations proved to be more accurate than the component method at low to moderate pressure ratios. However, at higher pressure ratios, convergence becomes more difficult and careful attention to the grid structure is required. Still, where the component method is a mature technology, the Navier-Stokes method shows potential for further refinement to the point where it may be used routinely for highly accurate predictions of separated flows.

Resources should be turned now to the development of better Navier-Stokes methods. This will require the implementation of better turbulence models, more computer memory, and, of course, higher computational speeds. Refinement of algorithms is also required so that the nozzle-lip problem may be handled without resort to artifices such as described in the text.

REFERENCES

1. Chang, P. K. *Separation of Flow*. Pergamon Press, New York (First Edition). 1970.

2. Bauer, R. C. and Fox, J. H. "An Application of the Chapman-Korst Theory to Supersonic Nozzle-Afterbody Flows." AEDC-TR-76-158 (AD-A035254), January 1977.

3. Fox, J. H. "A Generalized Base-Flow Analysis with Initial Boundary-Layer and Chemistry Effects." AEDC-TR-79-46 (AD-A072683), July 1979.

4. Fox, J. H. and Bauer, R. C. "Analytical Prediction of the Base Pressure Resulting from Hot, Axisymmetric Jet Interaction in Supersonic Flow." AIAA Paper 81-1898, AIAA Atmospheric Flight Mechanics Conference, Albuquerque, New Mexico, August 1981.

5. Chapman, A. J. and Korst, H. H. "Free Jet Boundary with Consideration of Initial Boundary Layer." *Proceedings of the Second U. S. National Congress of Applied Mechanics*, The American Society of Mechanical Engineers, New York, 1954, pp. 723-731.

6. Korst, H. H., Chow, W. L., and Zumwalt, G. W. "Research on Transonic and Supersonic Flow of a Real Fluid at Abrupt Increases in Cross Section — Final Report." ME Technical Report 392-5, University of Illinois, Urbana, December 1959.

7. Hahn, M., Rubbert, P. E., and Mahal, Avtar S. "Evaluation of Separation Criteria and Their Application to Separated Flow Analysis." AFFDL-TR-72-145, January 1973.

8. Bauer, R. C. "An Analysis of Two-Dimensional Laminar and Turbulent Compressible Mixing, *AIAA Journal*, Vol. 4, No. 3, March 1966, pp. 392-395.

9. Strickland, J. H., Simpson, R. L., and Barr, P. W. "Features of a Separating Turbulent Boundary Layer in the Vicinity of Separation." *Journal of Fluid Mechanics*, Vol. 79, Part 3, March 1977, pp. 553-594.

10. Strickland, J. H. and Simpson, R. L. "The Separating Turbulent Boundary Layer: An Experimental Study of an Airfoil Type Flow." Technical Report WT-2, Southern Methodist University Thermal and Fluid Sciences Center, August 1973.

11. Petri, Fred. "The Addition of Secondary Shock Capability and Modifications to the GASL Three-Dimensional Characteristics Program. Part I: Analysis and Results". General Applied Sciences Laboratory Report TR-653, (AD659808), August 1967.

12. Whitfield, D. L. "Integral Solution of Compressible Turbulent Boundary Layers Using Improved Velocity Profiles." AEDC-TR-78-42 (AD-A062946), December 1978.

13. James, C. R., Jr. "Aerodynamics of Rocket Plume Interactions at Supersonic Speeds." AIAA Paper No. 81-1905, AIAA Atmospheric Flight Mechanics Conference, Albuquerque, New Mexico, August 1981.

14. Agrell, J. and White, R. A. "An Experimental Investigation of Supersonic Axisymmetric Flow over Boattails Containing a Centered Propulsive Jet." FAA Technical Note AU-93, 1974.

15. Baldwin, B. and Lomax, H. "Thin-Layer Approximation and Algebraic Model for Separated Turbulent Flows." AIAA Paper 78-257, AIAA 16th Aerospace Sciences Meeting, Huntsville, Alabama, January 1978.

16. Johnson, D. A. and King, L. S. "A New Turbulence Closure Model for Boundary Layer Flows with Strong Adverse Pressure Gradients and Separation." AIAA Paper 84-0175, AIAA 22nd Aerospace Sciences Meeting, Reno, Nevada, 1984.

17. Deiwert, G. S. "A Computational Investigation of Supersonic Axisymmetric Flow over Boattails Containing a Centered Propulsive Jet." AIAA Paper No. 83-0462, AIAA 21st Aerospace Sciences Meeting, Reno, Nevada, January 1983.

18. Pulliam, T. H. and Steger, J. L. "Implicit Finite-Difference Simulations of Three-Dimensional Compressible Flow." *AIAA Journal*, Vol. 18, No. 2, February 1980, pp. 159-167.

19. Thomas, P. D. "Numerical Method for Predicting Flow Characteristics and Performance of Nonaxisymmetric Nozzles, Part 2 — Applications." NASA Contractor Report 3264, Langley Research Center, Virginia, October 1980.

20. Benek, J. A. "Separated and Nonseparated Turbulent Flows about Axisymmetric Nozzle Afterbodies, Part II, Detailed Flow Measurements." AEDC-TR-79-22 (AD-A076458), October 1979.

21. Swanson, Charles R., Jr. "Numercial Solutions of the Navier-Stokes Equations for Transonic Afterbody Flows." NASA Technical Paper 1784, Langley Research Center, Virginia, December 1980.

22. Shang, J. S. and Hankey, W. L., Jr. "Numerical Solution for Supersonic Turbulent Flow over a Compression Ramp." *AIAA Journal*, Vol. 13, No. 10, October 1975, pp. 1368-1374.

23. Simmonds, James G. *A Brief on Tensor Analysis*. New York, Springer-Verlag, 1982.

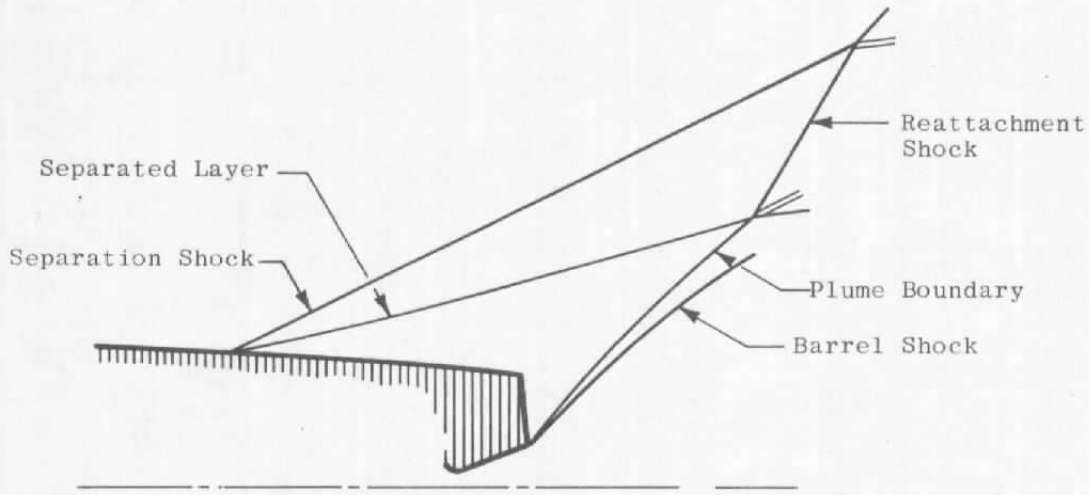

Figure 1. Schematic of plume interaction.

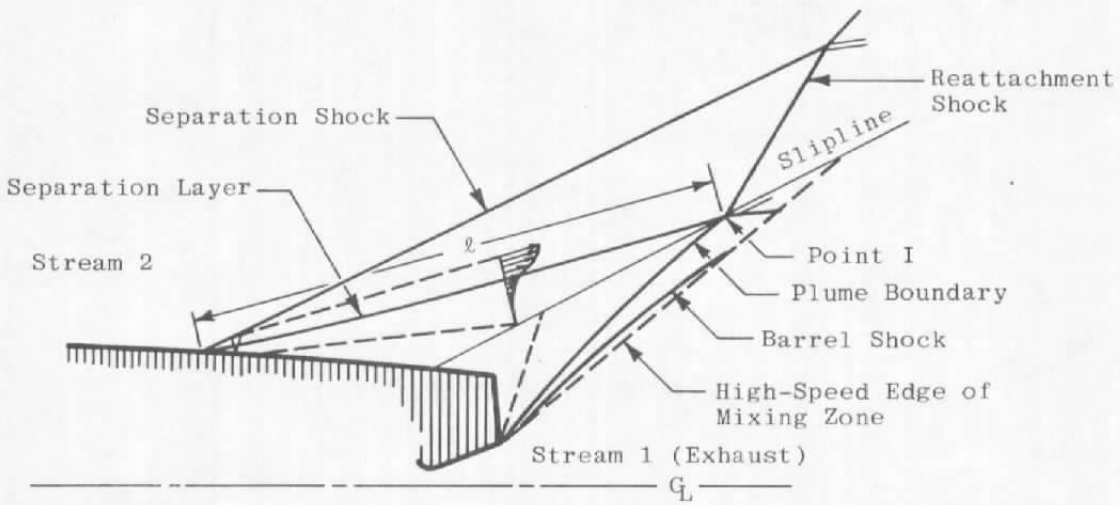

Figure 2. Interaction showing shear-layer model.

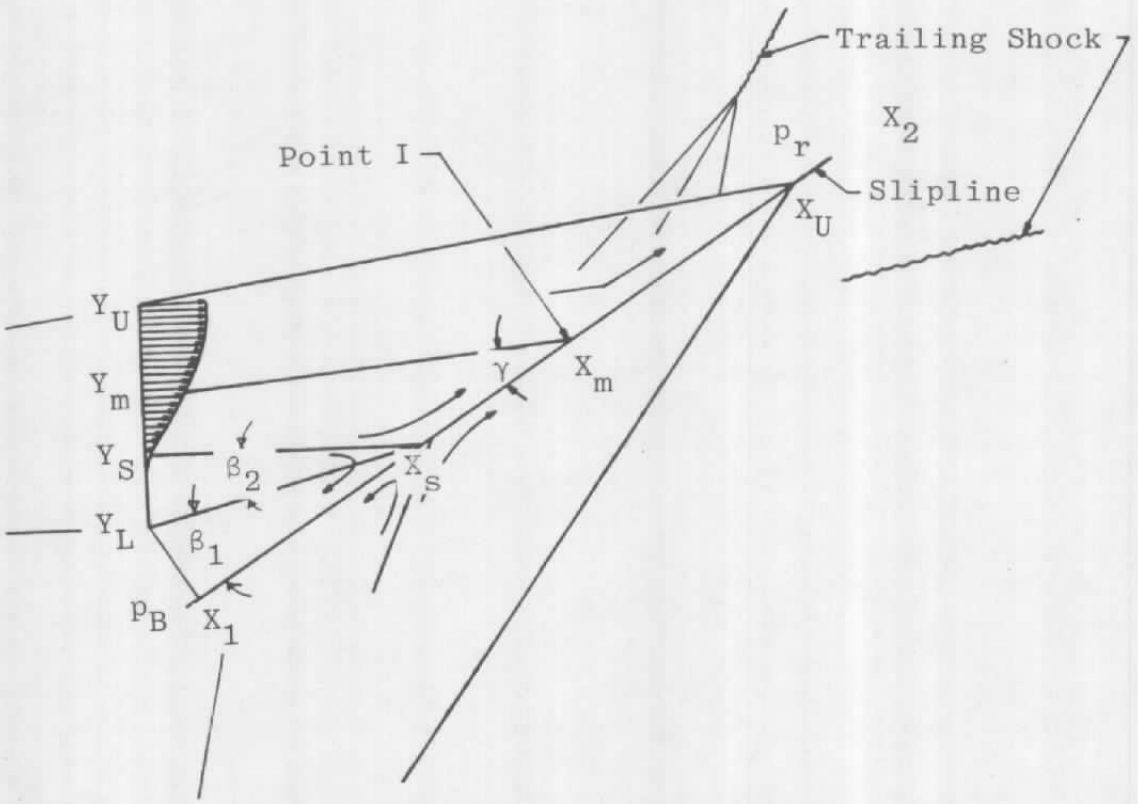

Figure 3. Details of recompression region.

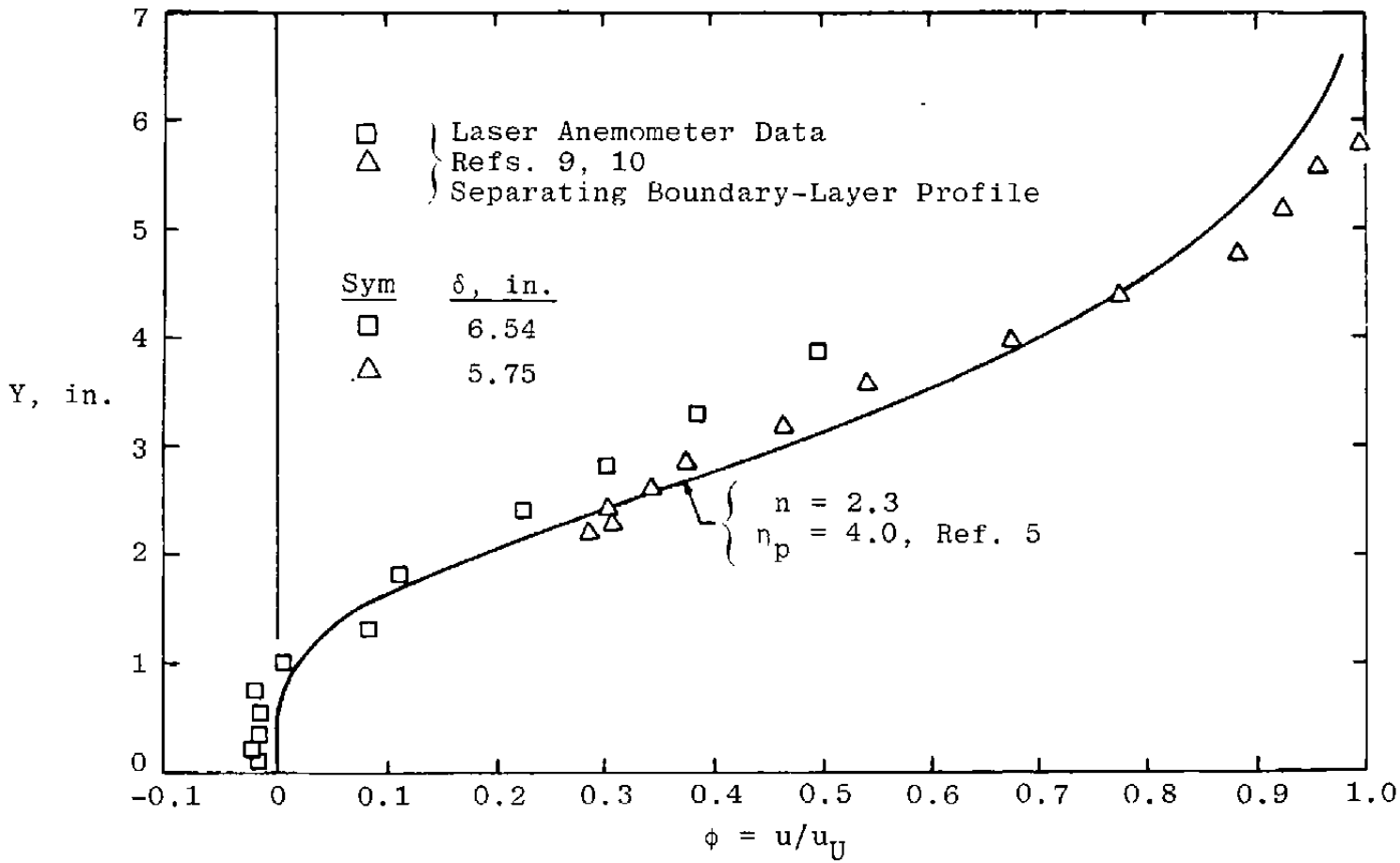

Figure 4. Typical separated boundary-layer profile.

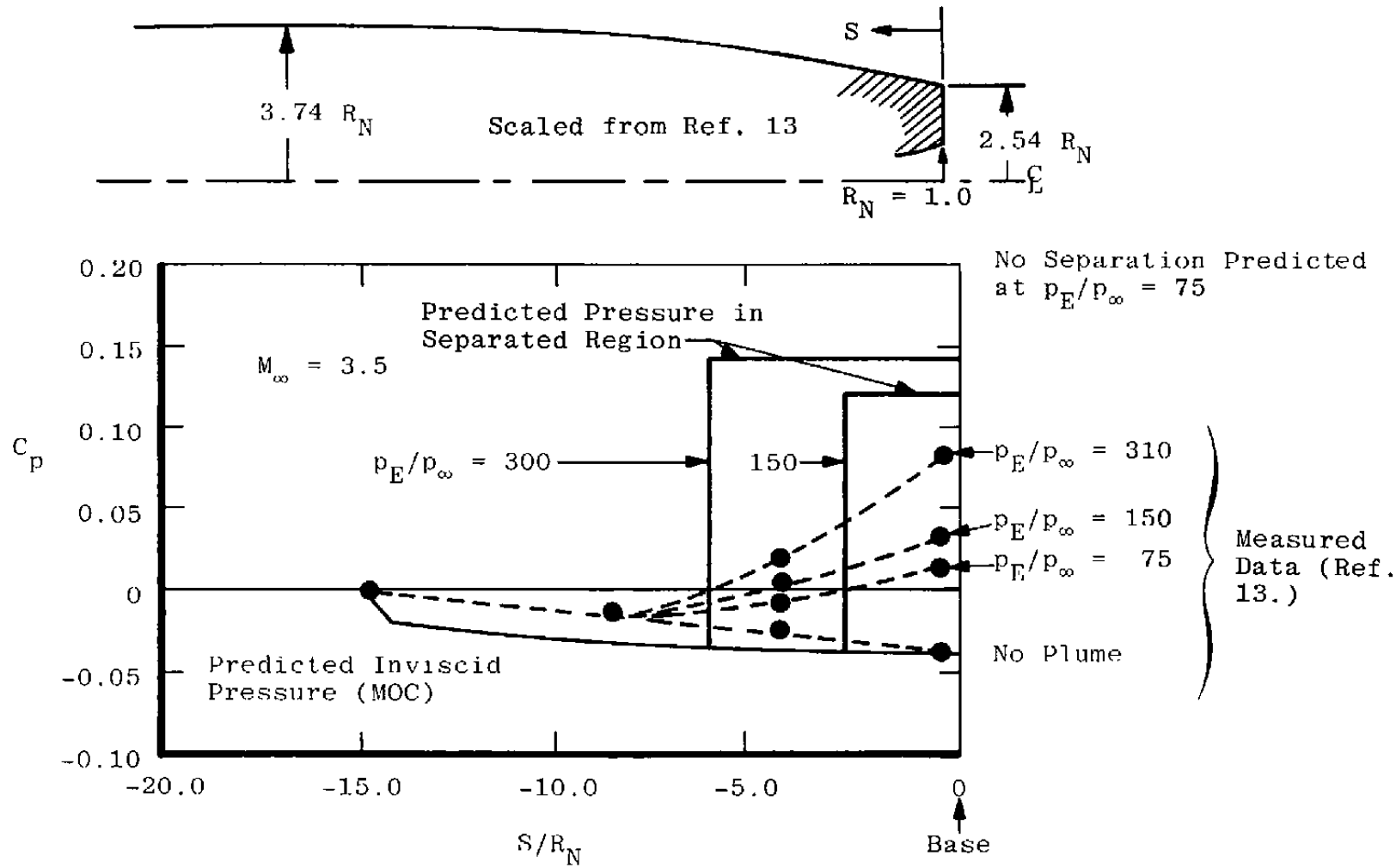

Figure 5. Afterbody pressure distribution, component method.

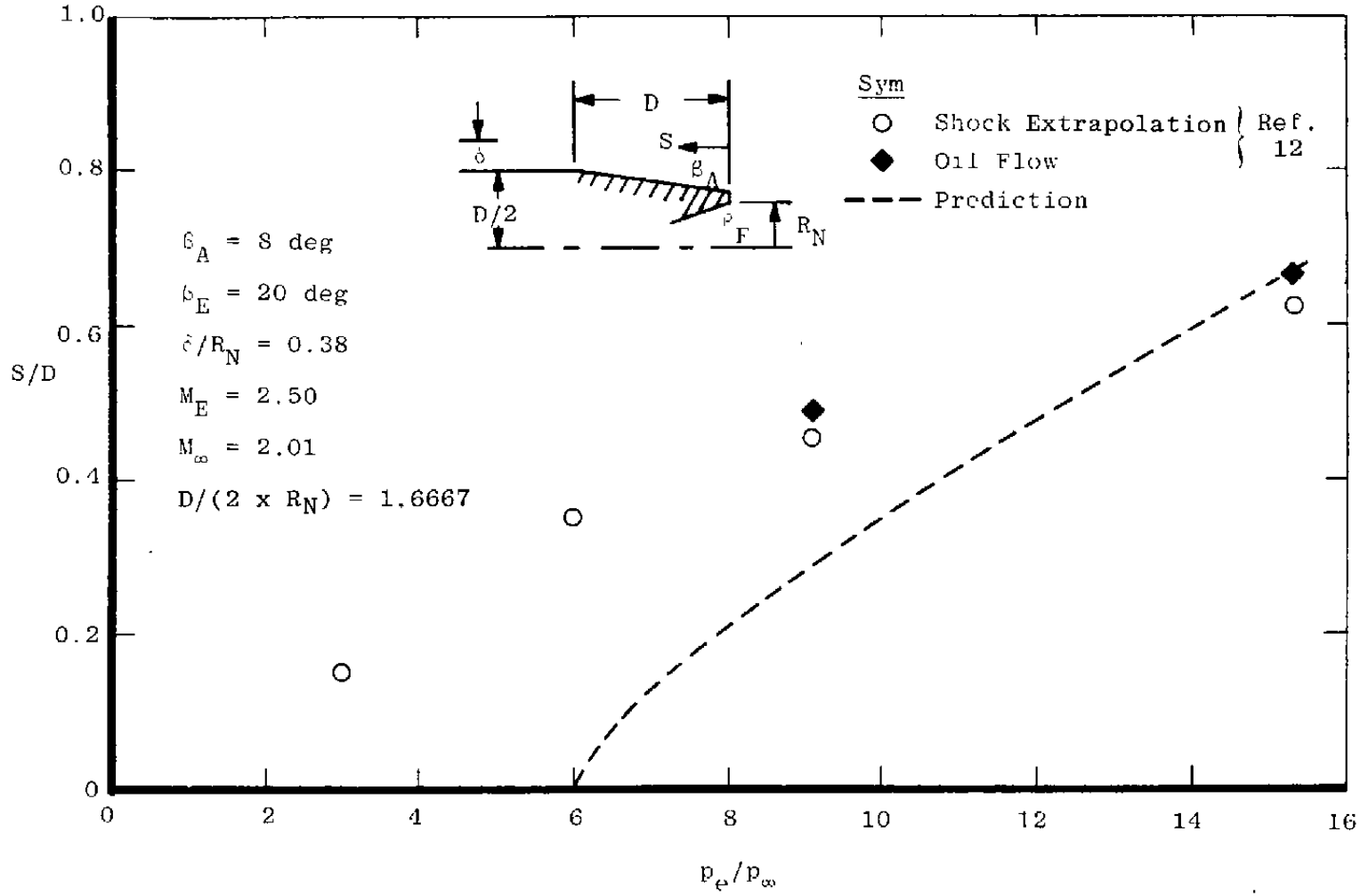

Figure 6. Prediction of separation extent, component method.

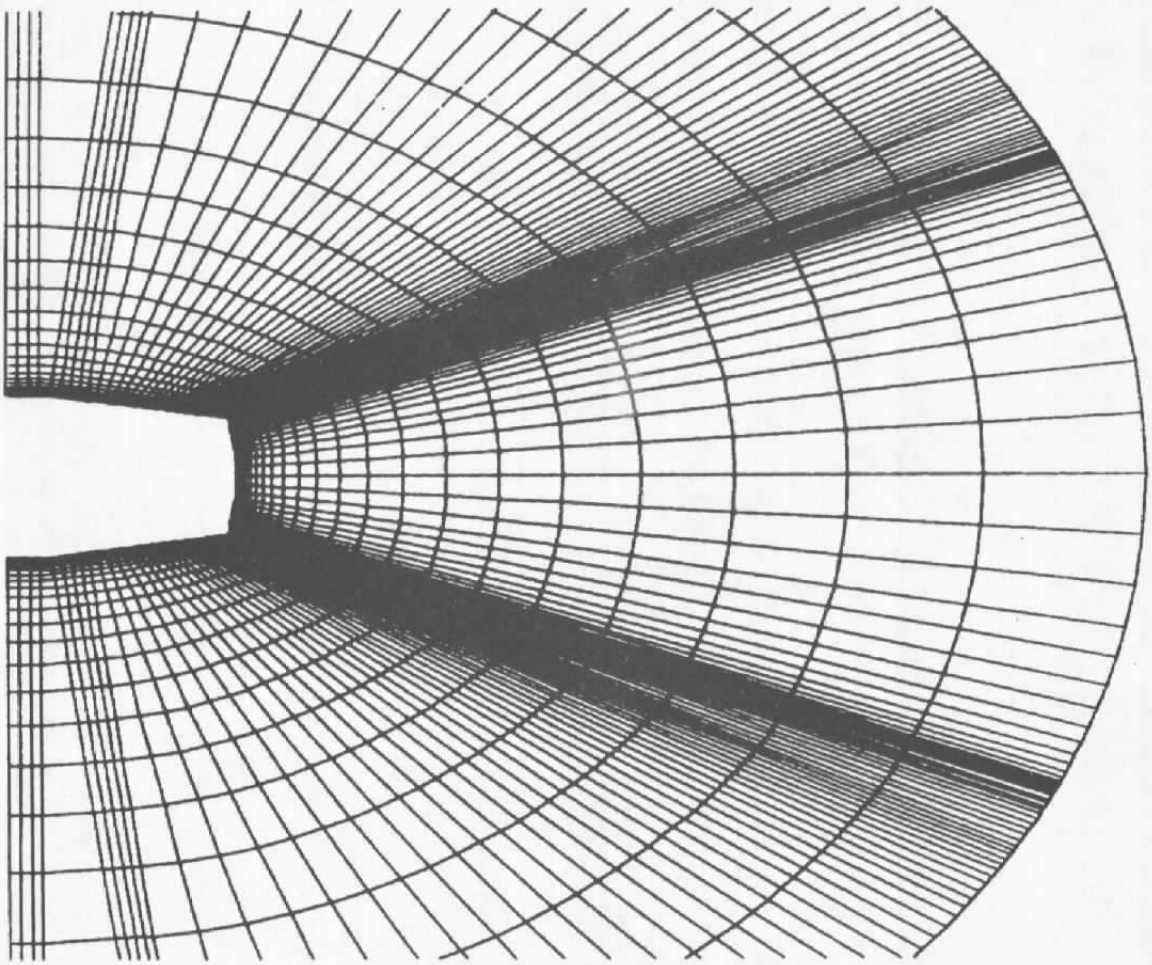

Figure 7. Computational grid.

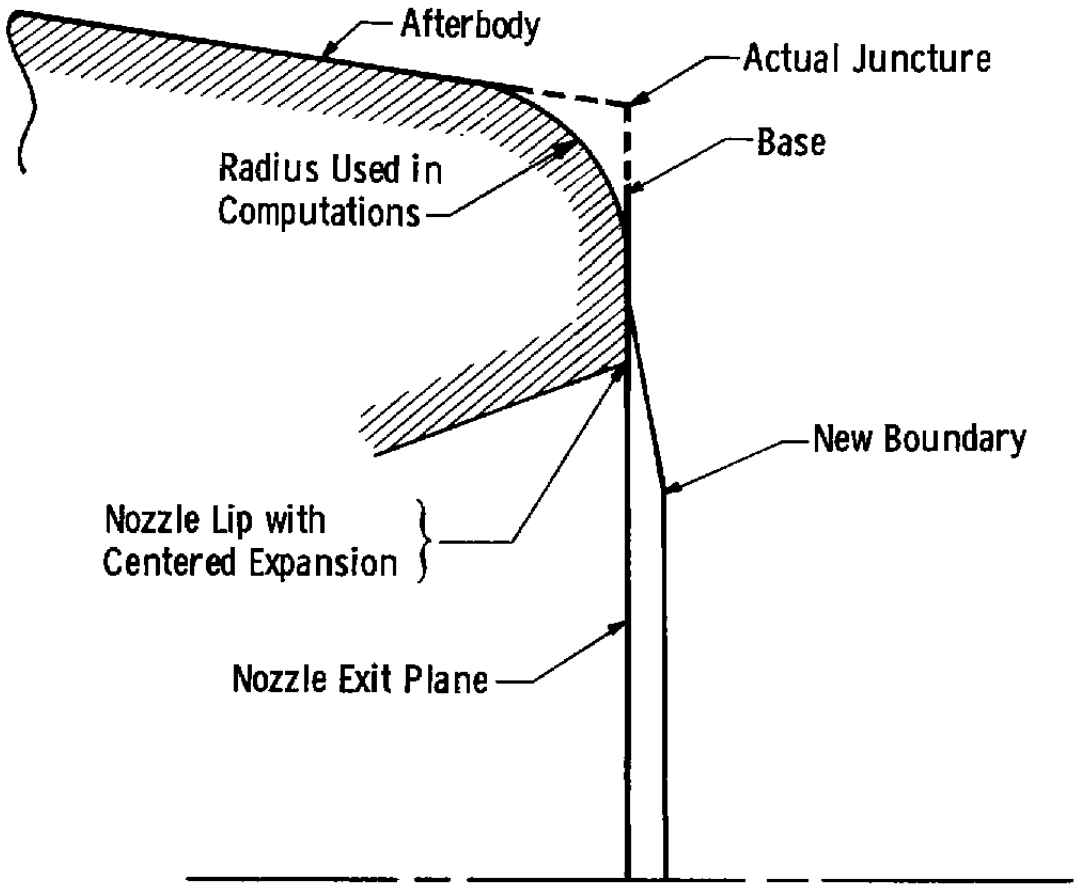

Figure 8. Schematic of base region.

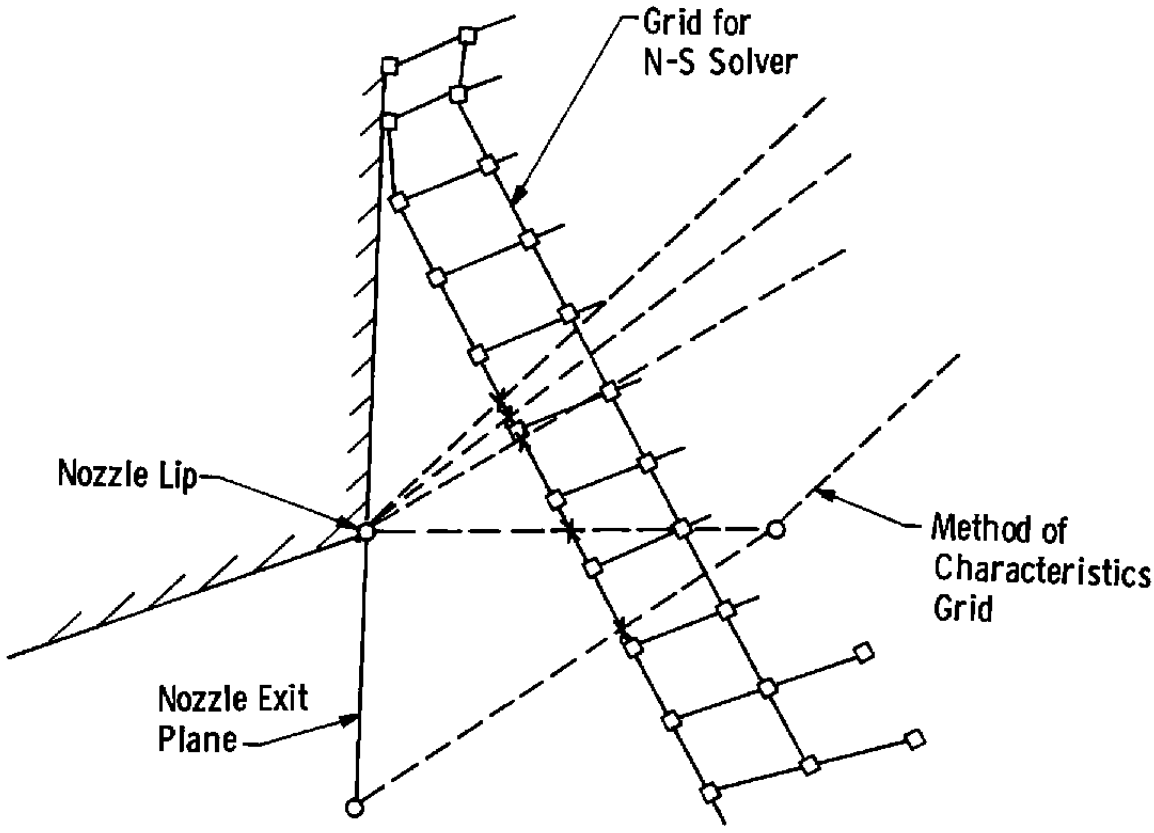

Figure 9. Overlapping grids.

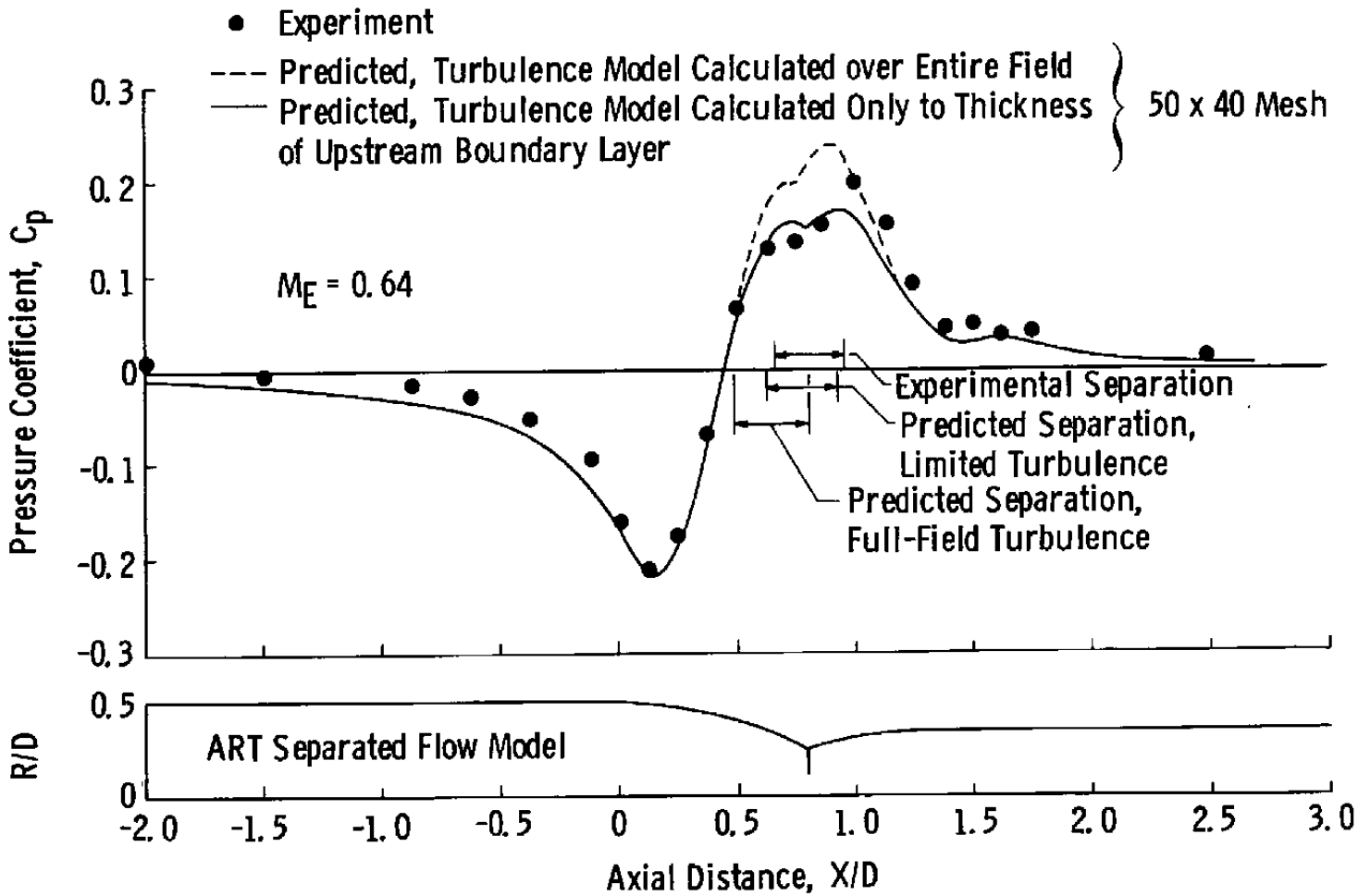

Figure 10. ART solid-sting comparison.

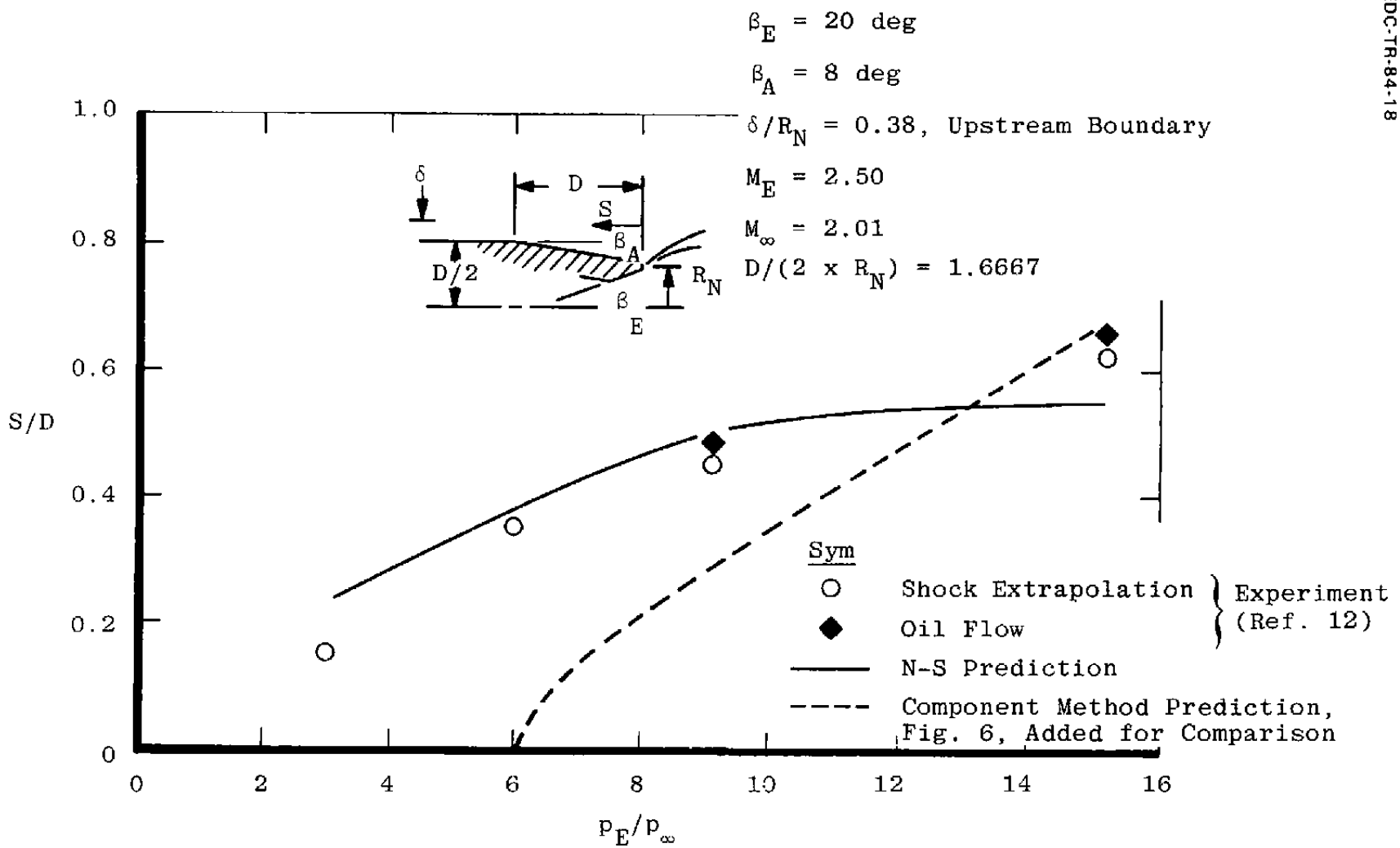

Figure 11. Prediction of separation extent, Navier-Stokes method.

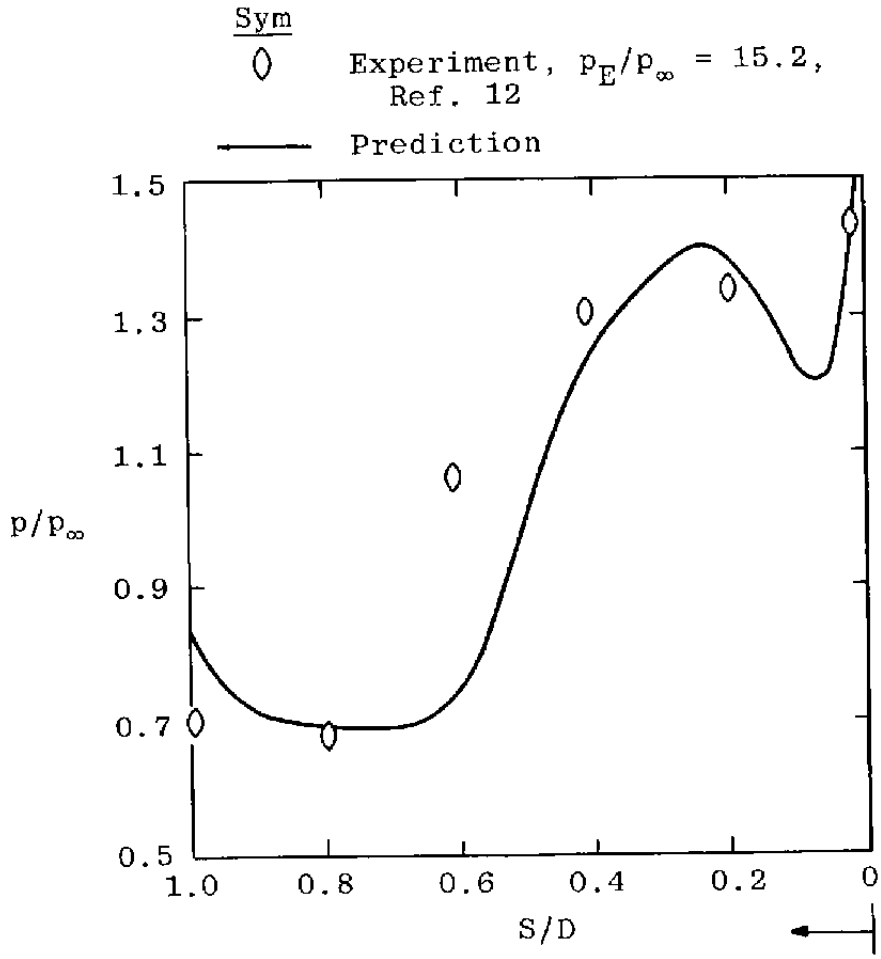

a. p_E/p_∞ = 15.2

Figure 12. Afterbody pressure distribution.

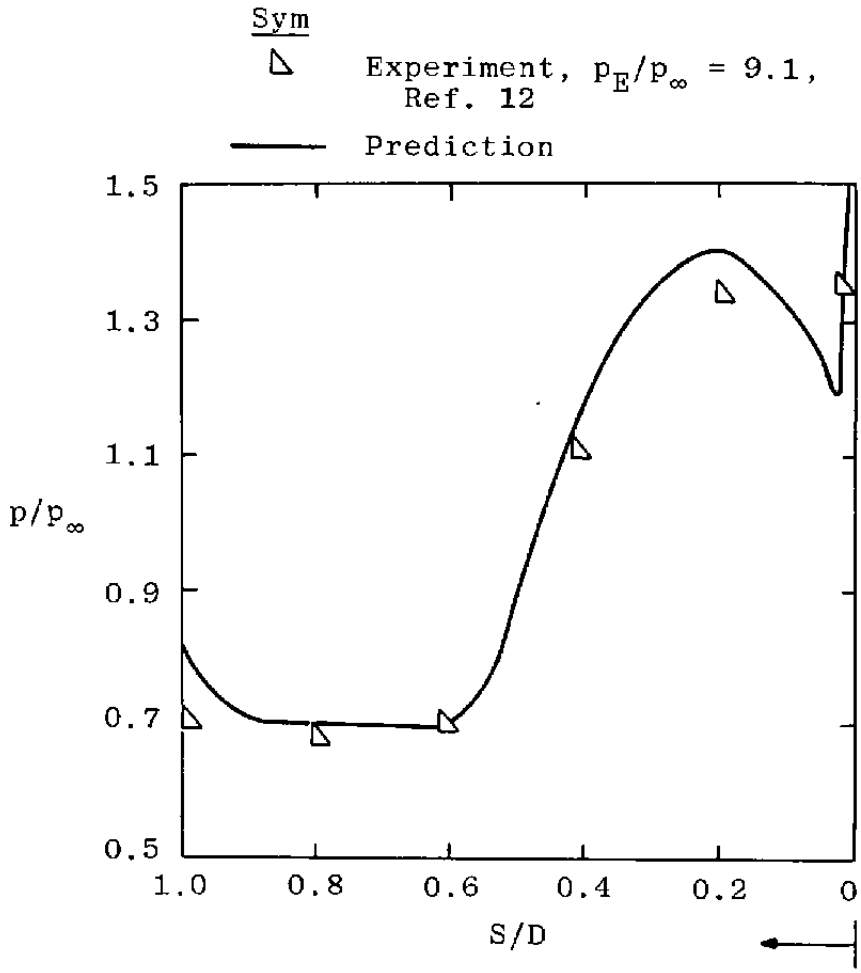

b. p_E/p_∞ = 9.1

Figure 12. Continued.

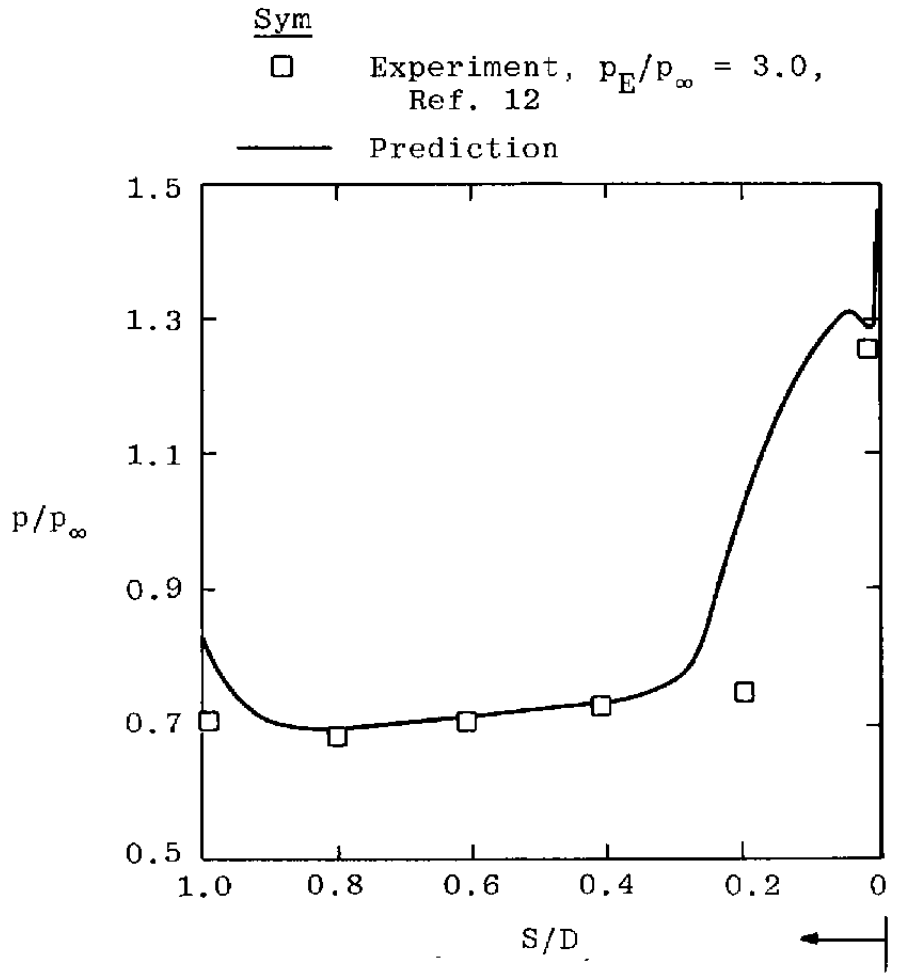

c. p_E/p_∞ = 3.0

Figure 12. Concluded.

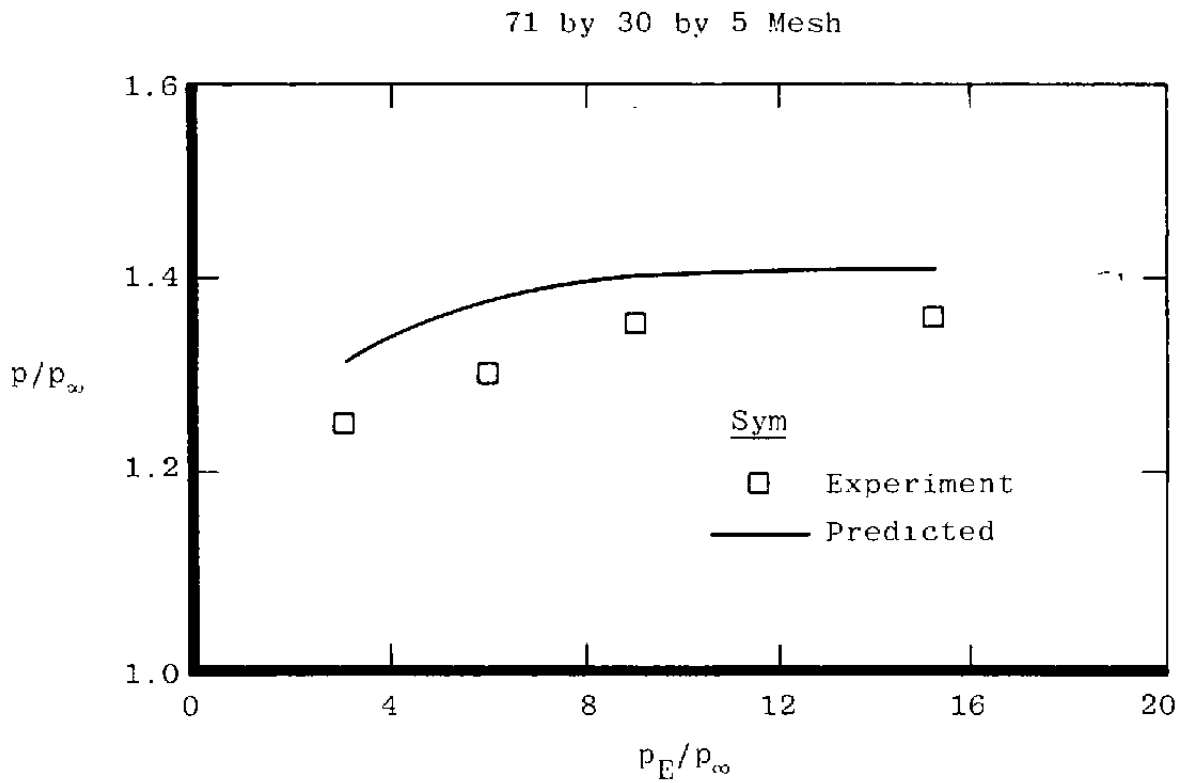

Figure 13. Plateau pressure comparison.

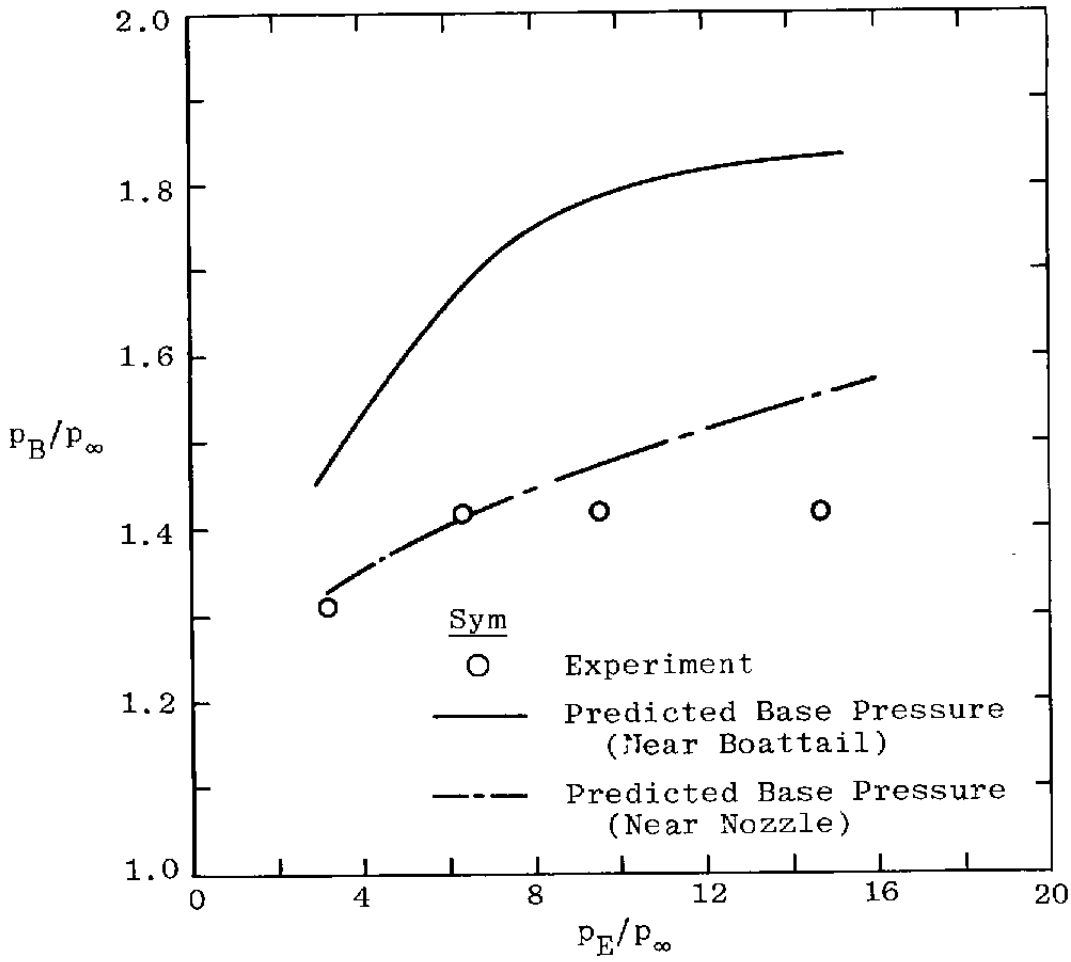

Figure 14. Base pressure comparison.

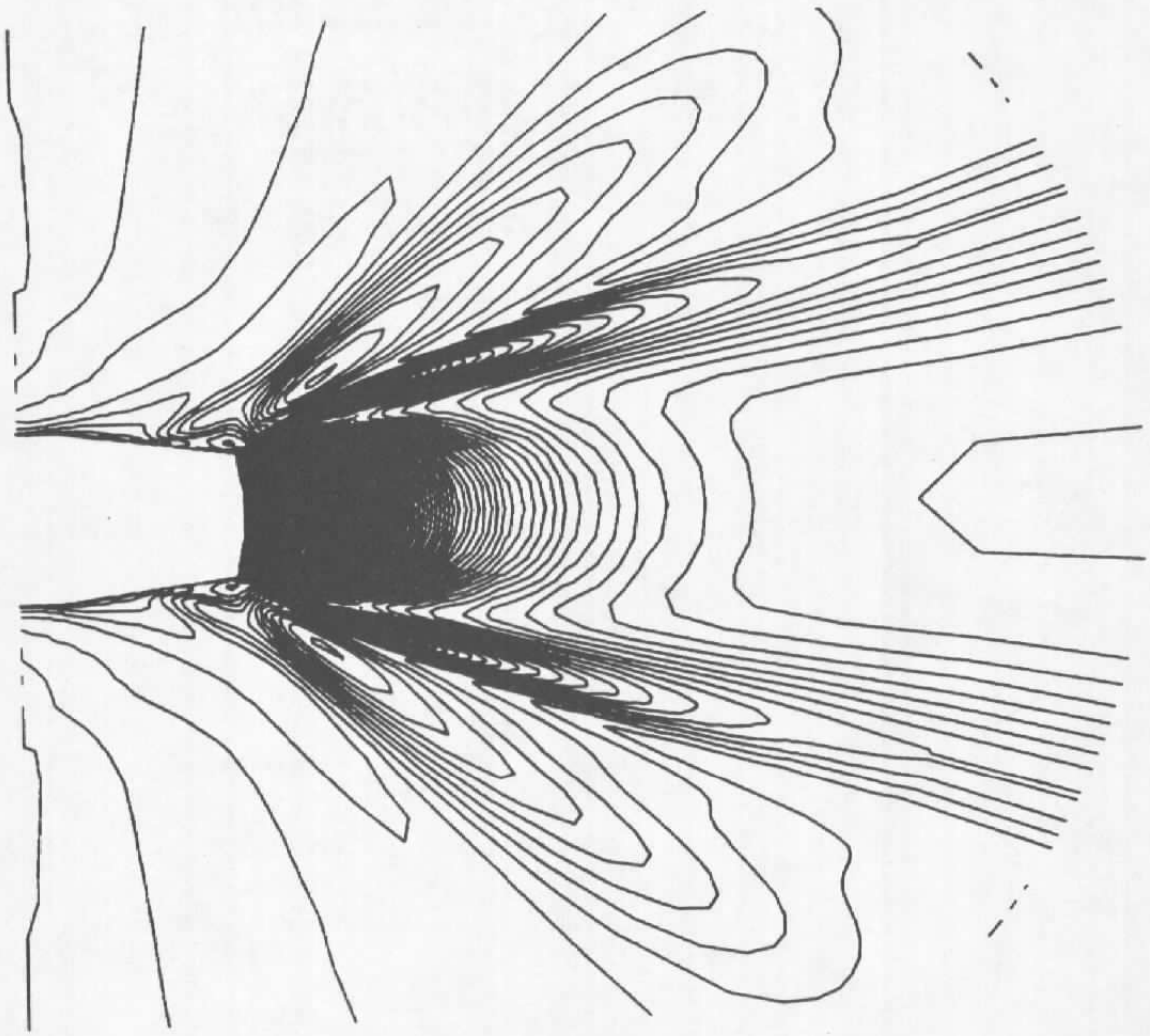

Figure 15. Density contour, $p_E/p_\infty = 15.2$.

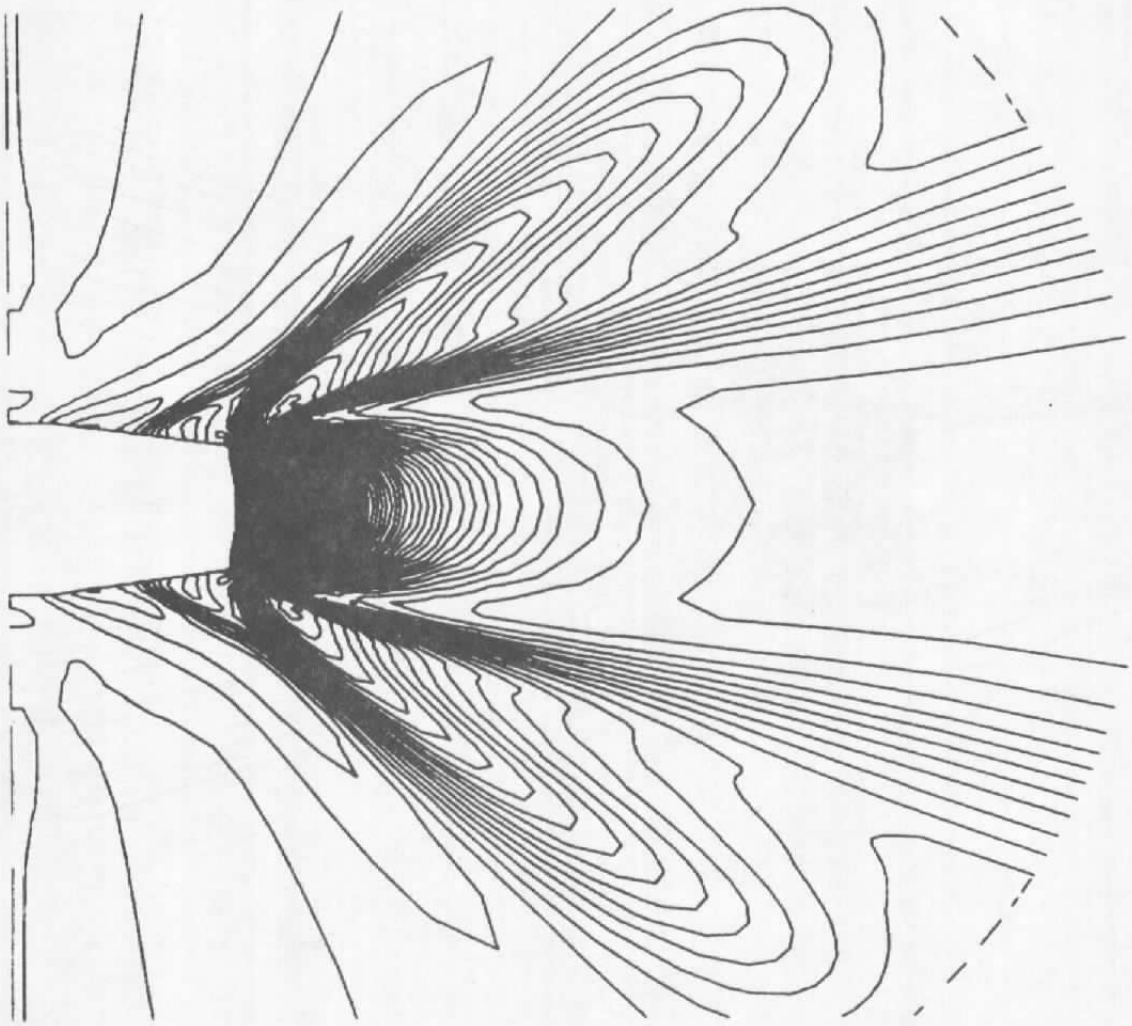

Figure 16. Pressure contour, $p_E/p_\infty = 15.2$.

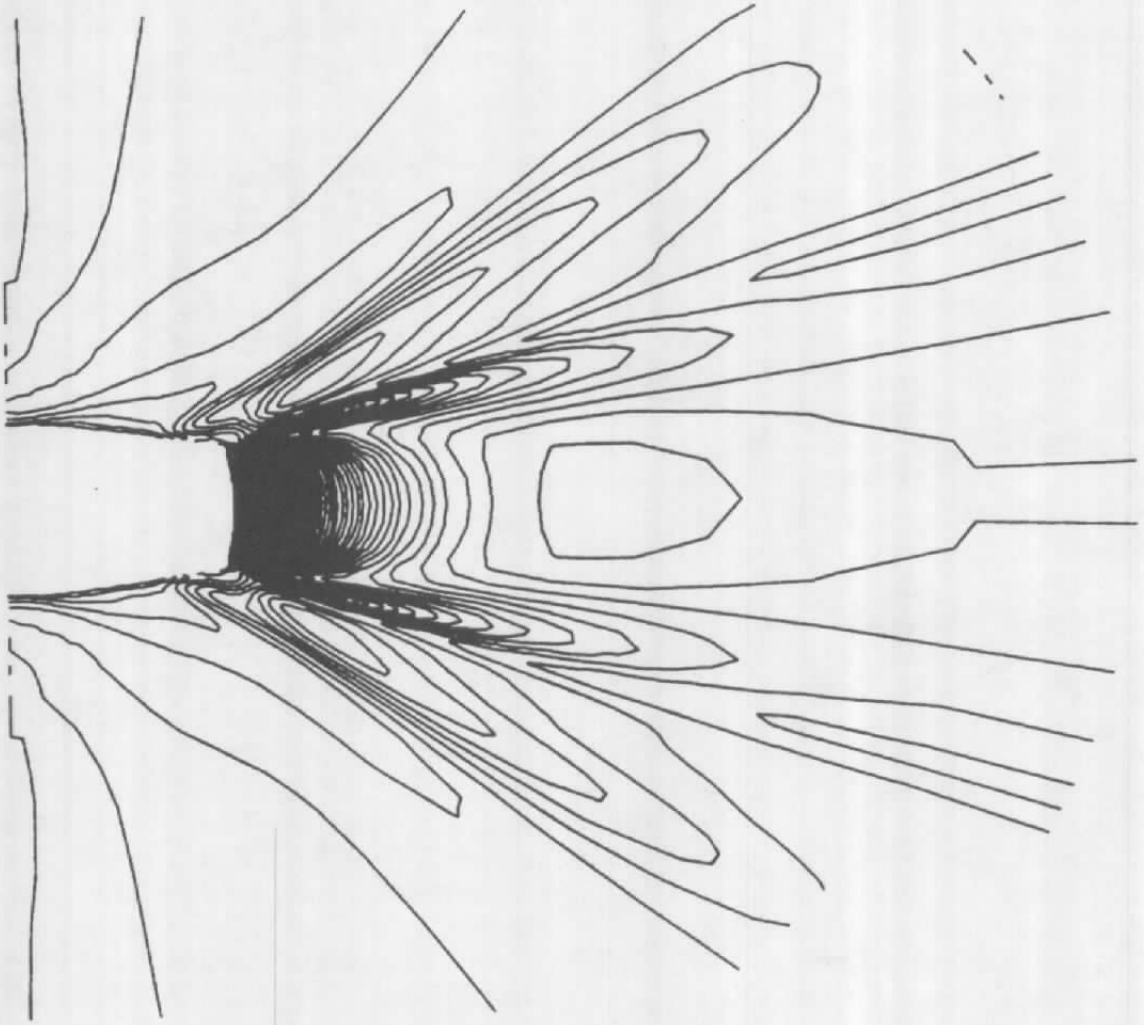

Figure 17. Density contour, $p_E/p_\infty = 6.0$.

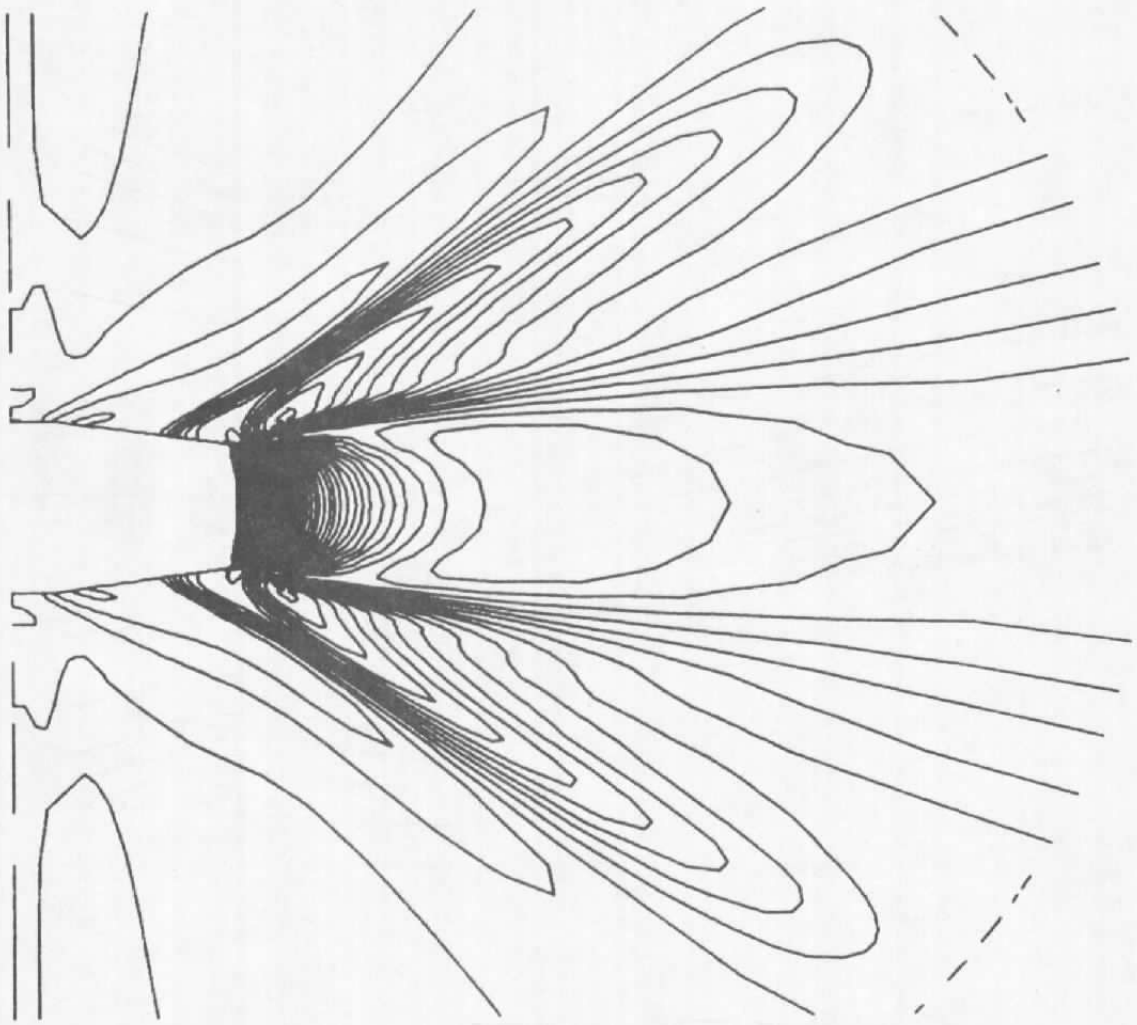

Figure 18. Pressure contour, $p_E/p_\infty = 6.0$.

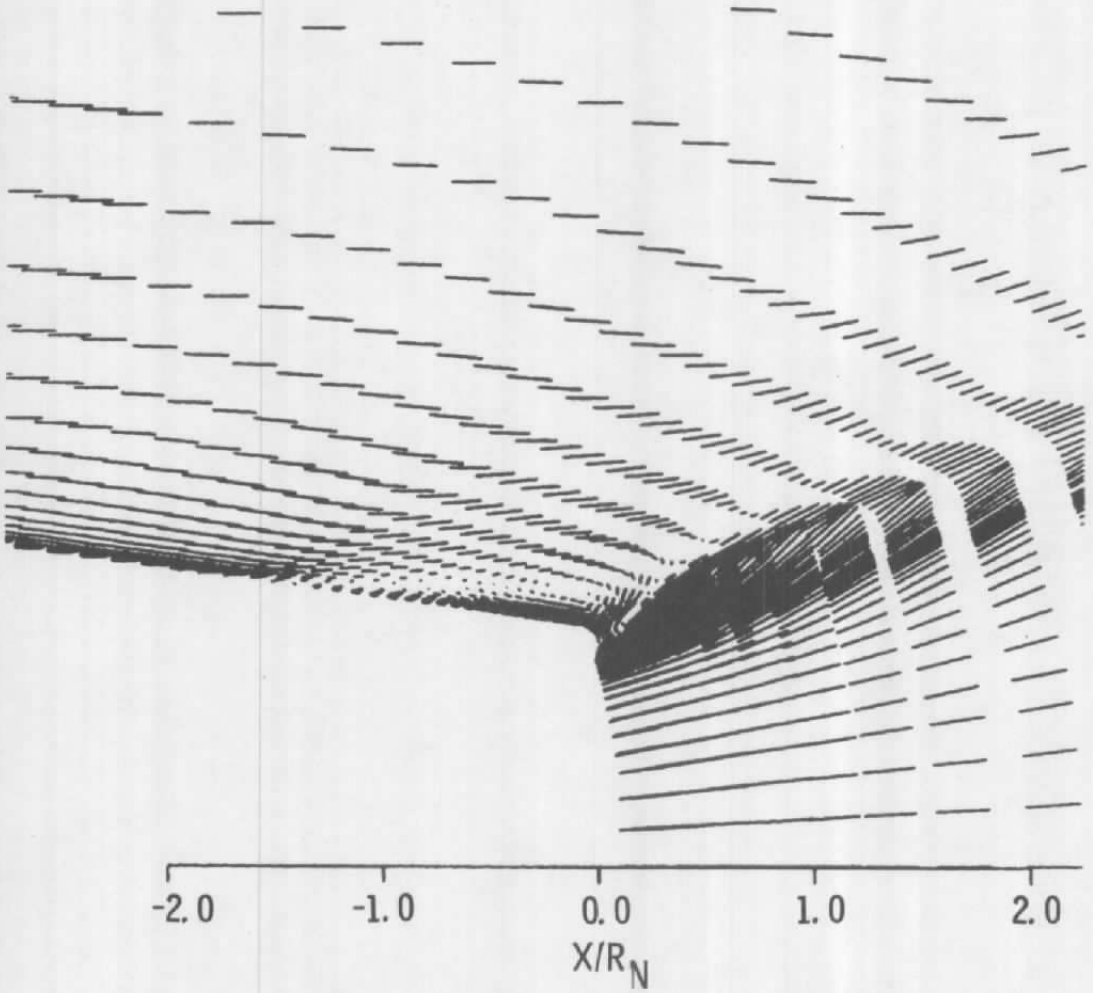

Figure 19. Velocity vectors, $p_E/p_\infty = 6.0$.

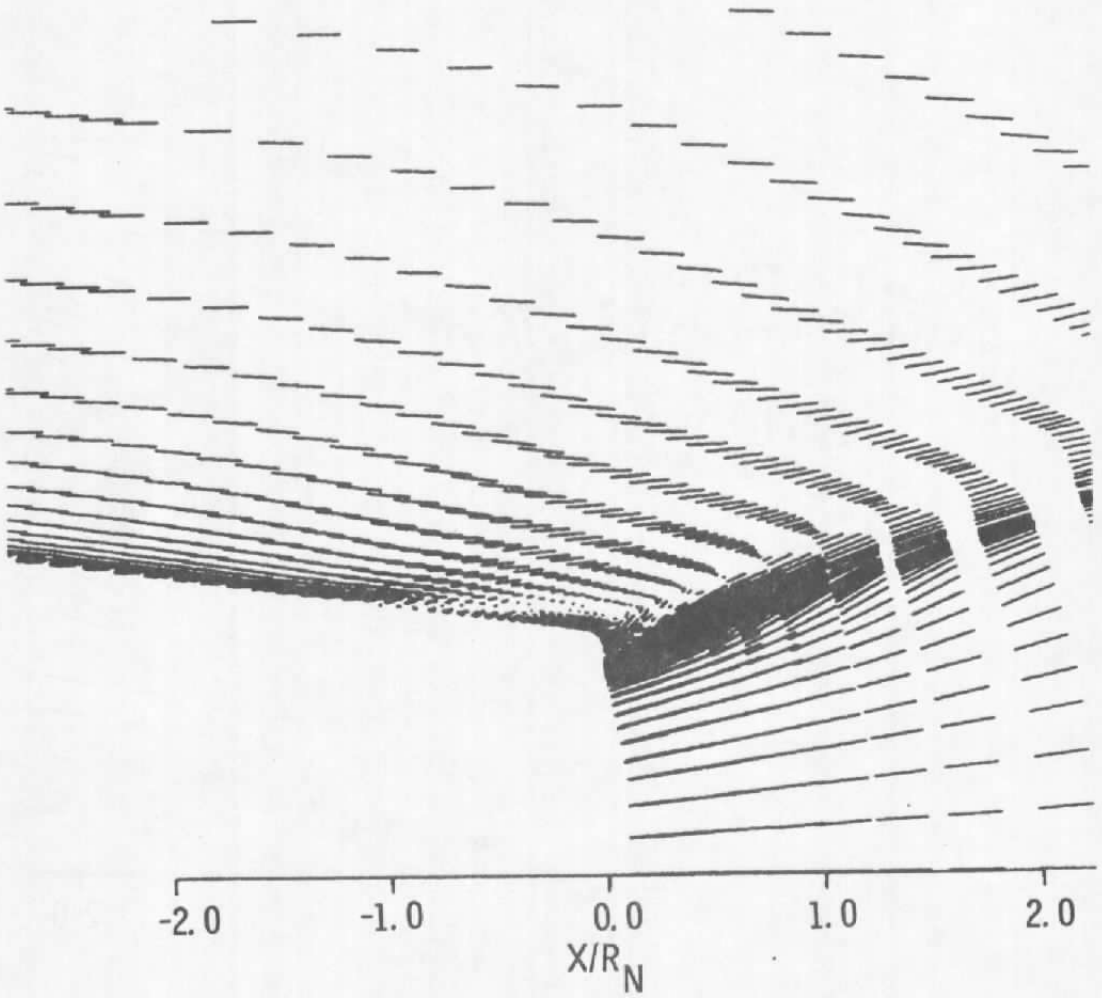

Figure 20. Velocity vectors, $p_E/p_\infty = 15.2$.

APPENDIX A
TRANSFORMATION TO CURVILINEAR COORDINATES

Consider the general form of the dimensionless conservation equations in Cartesian coordinates.

$$\partial_t q + \partial_x E + \partial_y F + \partial_z G = R_e^{-1} (\partial_x R + \partial_y S + \partial_z T) \tag{A-1}$$

where $\partial_x \equiv \partial/\partial x$,etc.

Define vectors such that

$$\vec{V} = [q, E, F, G] \equiv [V^1, V^2, V^3, V^4]$$

$$\vec{W} = [R, S, T] \equiv [W^1, W^2, W^3]$$

Equation (A-1) may now be written in divergence form as

$$\nabla \cdot \vec{V} = \frac{1}{R_e} \nabla \cdot \vec{W} \tag{A-2}$$

From tensor analysis, viz. Ref. 23, in general coordinates

$$\nabla \cdot \vec{V} = J\partial_{x^i} (J^{-1} V^i)$$

and

$$\nabla \cdot \vec{W} = J\partial_{x^i} (J^{-1} W^i)$$

where the Jacobian notation, J, is inverted to conform with Pulliam and Steger. Elements V^i and W^i are the contravariant components of $\vec{V}$ and $\vec{W}$. The divergence is invariant under transformation as are the vectors; therefore, the only effort required is in determining these vector components in the curvilinear system.

Contravariant vectors components transform from Cartesian [t,x,y,z] to curvilinear [τ, ξ, η, ζ] coordinates as

$$\bar{V}^1 = \delta_t \tau V^1$$

$$\bar{V}^2 = \partial_t \xi V^1 + \partial_x \xi V^2 + \partial_y \xi V^3 + \partial_z \xi V^4 \tag{A-3}$$

$$\bar{V}^3 = \partial_t \eta V^1 + \partial_x \eta V^2 + \partial_y \eta V^3 + \partial_z \eta V^4$$

$$\bar{V}^4 = \partial_t \zeta V^1 + \partial_x \zeta V^2 + \partial_y \zeta V^3 + \partial_z \zeta V^4$$

In the same way, $W^i \rightarrow \bar{W}^i$

also

$$J = \begin{vmatrix} \tau_t & 0 & 0 & 0 \\ \xi_t & \xi_x & \xi_y & \xi_z \\ \eta_t & \eta_x & \eta_y & \eta_z \\ \zeta_t & \zeta_x & \zeta_y & \zeta_z \end{vmatrix}$$

where $\xi_x \equiv \partial_x \xi$, etc.

From Eqs. (A-2) and (A-3)

$$\partial_\tau \bar{q} + \partial_\xi \bar{E} + \partial_\eta \bar{F} + \partial_\zeta \bar{G} = R_e^{-1}(\partial_\xi \bar{R} + \partial_\eta \bar{S} + \partial_\zeta \bar{T}) \qquad \text{(A-4)}$$

where

$$\bar{q} \equiv J^{-1} \bar{V}^1, \bar{E} \equiv J^{-1} \bar{V}^2, \bar{F} \equiv J^{-1} \bar{V}^3, \text{ and } \bar{G} \equiv J^{-1} \bar{V}^4$$

and

$$\bar{R} \equiv J^{-1} \bar{W}^1, \bar{S} \equiv J^{-1} \bar{W}^2, \bar{T} \equiv J^{-1} \bar{W}^3$$

The form of the conservation equations that is usually shown is obtained by substituting the variables for the vector components into Eq. (A-4).

For example, consider the ξ momentum equation. The Cartesian components are

$$V^1 \equiv q \equiv \varrho u, V^2 \equiv E \equiv \varrho u^2 + p, V^3 \equiv F \equiv \varrho v\theta, V^4 \equiv G \equiv \varrho uw$$

$$W^1 \equiv R \equiv \tau_{xx}, W^2 \equiv S \equiv \tau_{xy}, W^3 \equiv T \equiv \tau_{xz}$$

These are substituted into Eqs. (A-3). Then Eqs. (A-3) are substituted into Eq. (A-4).

The left-hand side of Eq. (A-4) becomes

$$\frac{\partial J^{-1}\,\varrho u}{\partial \tau} + \frac{\partial J^{-1}\,\xi_t\,\varrho u}{\partial \xi} + \frac{\partial J^{-1}\,\xi_x(\varrho u^2 + p)}{\partial \xi} + \frac{\partial J^{-1}\,\xi_y\,(\varrho uv)}{\partial \xi}$$

$$+ \frac{\partial J^{-1}\,\xi_z\,(\varrho uw)}{\partial \xi} + \frac{\partial J^{-1}\eta_t\,\varrho u}{\partial \eta}$$

$$+ \frac{\partial J^{-1}\,\eta_x(\varrho u^2 + p)}{\partial \eta} + \frac{\partial J^{-1}\eta_y(\varrho uv)}{\partial \eta} + \frac{\partial J^{-1}\,\eta_z(\varrho uw)}{\partial \eta}$$

$$+ \frac{\partial J^{-1}\zeta_t\varrho u}{\partial \zeta} + \frac{\partial J^{-1}\zeta_x(\varrho u^2 + p)}{\partial \zeta} + \frac{\partial J^{-1}\zeta_y(\varrho uv)}{\partial \zeta}$$

$$+ \frac{\partial J^{-1}\zeta_z(\varrho uw)}{\partial z} = \text{RHS}$$

Letting

$$U = \xi_t + \xi_x u + \xi_y v + \xi_z w$$

$$U = \eta_t + \eta_x u + \eta_y v + \eta_z w$$

$$W = \zeta_t + \zeta_x u + \zeta_y v + \zeta_z w$$

we get

$$\frac{\partial J^{-1}\varrho u}{\partial \tau} + \frac{\partial J^{-1}(\varrho uU + \xi_x p)}{\partial \xi} + \frac{\partial J^{-1}(\varrho uV + \eta_x p)}{\partial \eta} + \frac{\partial J^{-1}(\varrho uW + \zeta_x p)}{\partial \zeta} = \text{RHS}$$

and

$$\text{RHS} = R_e^{-1}\,\partial_\xi J^{-1}\,(\xi_x\,\tau_{xx} + \xi_y\tau_{xy} + \xi_z\tau_{xz}) + \partial_\eta J^{-1}(\eta_x\tau_{xx} + \eta_y\tau_{xy} + \eta_z\tau_{xz})$$

$$+ \partial_\zeta J^{-1}(\zeta_x\tau_{xx} + \zeta_y\tau_{xy} + \zeta_z\tau_{xz})$$

or for the thin-layer approximation:

$$\text{RHS} = R_e^{-1}\partial_\zeta J^{-1}(\zeta_x\tau_{xx} + \zeta_y\tau_{xy} + \zeta_z\tau_{xz})$$

The other conservation equations transform as easily.

NOMENCLATURE

a	Sound speed
C_p	Static pressure coefficient
c_p	Specific heat at constant pressure
e	Total energy
H	Total enthalpy
k	Effective thermal conductivity, $k = c_p (\mu_M/P_r + \mu_t/0.9)$
L	Body length
ℓ	Length of mixing region; mixing length in turbulence model
ℓ_{eff}	Effective mixing length
ℓ_{vir}	Virtual mixing length
M	Mach number
n	Inverse of power-law exponent
p	Static pressure
P_r	Prandtl number
R	Radius from axis of symmetry
$\bar{R}$	Average radius
Re_u	Unit Reynolds number
U	Velocity of high-speed edge of shear layer in direction of shear layer
u	Velocity component in Cartesian x direction; velocity in direction of development shear layer

U, V, W	Contravariant velocity components
v, w	Velocity component in Cartesian y and z directions, respectively
X	Coordinate along slipline in recompression region
x	Cartesian axial coordinate or mixing coordinate in direction of developing mixing layer
y	Cartesian coordinate transverse to x coordinate
β	Angle between slipline and mixing layer, Fig. 3; also used for nozzle and afterbody angles
δ	Boundary-layer thickness
γ	Ratio of specific heats
ζ	Curvilinear coordinate approximately normal to body, also boundary-layer coordinate, y/δ
η	Dimensionless mixing variable; body-conforming curvilinear coordinate in azimuthal direction
η_p	Dimensionless position parameter, $\sigma\delta/\ell$
ϕ	Velocity ratio in shear layer, u/U
τ	Shear stress; time
μ	Effective viscosity: molecular + turbulent, except when subscripted
μ_t	Turbulent viscosity
μ_M	Molecular viscosity
ξ	Body-conforming curvilinear coordinate in flow direction
ϱ	Density

σ	Mixing or spreading parameter
σ_0	Incompressible σ, a reference value
ω	Vorticity

SUBSCRIPTS

1	Beginning of recompression; also upstream of shock wave
2	End of recompression; also downstream of separating shock wave
B	Separated region; base region
D	Dividing streamline
E	Nozzle exit condition
∞	Free-stream condition
L	Low-speed edge of mixing layer
M	Molecular
m	Inviscid boundary with respect to origin of mixing profile
N	Nozzle
r	Downstream of recompression shock wave
S	Stagnating streamline
S1	Stream 1 (jet plume)
S2	Stream 2 (outer stream)
T	Total condition
U	High-speed edge of mixing layer